Tuning the Functionality of Designer Translating Organelles with Orthogonal tRNA Synthetase/tRNA Pairs

Mikhail E. Sushkin [1,2], Marius Jung [1,3] and Edward A. Lemke [1,4,*]

*1 - **Biocenter,** Johannes Gutenberg University Mainz, Hanns-Dieter-Hüsch-Weg 17, 55128 Mainz, Germany*
*2 - **International PhD Programme of the Institute of Molecular Biology (IMB) gGmbH,** Hanns-Dieter-Hüsch-Weg 17, 55128 Mainz, Germany*
*3 - **Biocenter,** IMPRS on Cellular Biophysics, Johannes Gutenberg University Mainz, Hanns-Dieter-Hüsch-Weg 17, 55128 Mainz, Germany*
*4 - **Institute of Molecular Biology (IMB) gGmbH,** Ackermannweg 4, 55128 Mainz, Germany*

Correspondence to Edward A. Lemke: *Biocenter, Johannes Gutenberg University Mainz, Hanns-Dieter-Hüsch-Weg 17, 55128 Mainz, Germany. *edlemke@uni-mainz.de* *(E.A. Lemke)*
https://doi.org/10.1016/j.jmb.2024.168728
Edited by Sheena Radford

Abstract

Site-specific incorporation of noncanonical amino acids (ncAAs) can be realized by genetic code expansion (GCE) technology. Different orthogonal tRNA synthetase/tRNA (RS/tRNA) pairs have been developed to introduce a ncAA at the desired site, delivering a wide variety of functionalities that can be installed into selected proteins. Cytoplasmic expression of RS/tRNA pairs can cause a problem with background ncAA incorporation into host proteins. The application of orthogonally translating organelles (OTOs), inspired by the concept of phase separation, provides a solution for this issue in mammalian cells, allowing site-specific and protein-selective ncAA incorporation. So far, only *Methanosarcina mazei* (*Mm*) pyrrolysyl-tRNA synthetase (PylRS) has been used within OTOs, limiting the method's potential. Here, we explored the implementation of four other widely used orthogonal RS/tRNA pairs with OTOs, which, to our surprise, were unsuccessful in generating mRNA-selective GCE. Next, we tested several experimental solutions and developed a new chimeric phenylalanyl-RS/tRNA pair that enables ncAA incorporation in OTOs in a site-specific and protein-selective manner. Our work reveals unaccounted design constraints in the spatial engineering of enzyme functions using designer organelles and presents a strategy to overcome those *in vivo*. We then discuss current limitations and future directions of in-cell engineering in general and protein engineering using GCE specifically.

Introduction

Protein engineering aims to create new variants of proteins, which can be helpful for many medical and biological applications. Nature uses 20 canonical amino acids (AAs, up to 22 in some organisms capable of working both with selenocysteine and pyrrolysine, Pyl) for the synthesis of a tremendous number of proteins, utilizing different combinations of AAs' sequences and inserting diverse post-translational modifications. However, the scope of potential protein molecules can be even infinite if new noncanonical amino acids (ncAAs) are incorporated into the protein polymer chain. The technology, called genetic code expansion (GCE), provides an opportunity to install ncAAs at a selected site in a programmed way. An orthogonal aminoacyl-tRNA synthetase/tRNA (RS/tRNA) pair is typically used to drive the aminoacylation of the

tRNA with desired ncAA and to exploit further the charged tRNAs in the translation process of the protein of interest (POI). Most commonly, the selected site of the POI is encoded by an introduced stop codon to direct the incorporation of the ncAA of choice. Since the anticodon of the tRNAs charged with the ncAA is designed to recognize the introduced stop codon, they are called suppressor tRNAs (Figure 1A; see Refs.[1–4] for reviews). The important prerequisite for correct functionality of the whole RS/tRNA/ncAA system is its orthogonality with the components of the host translational machinery. This means that (1) an orthogonal RS should not recognize host tRNAs and canonical AAs for the aminoacylation reaction, (2) host RS should not charge the suppressor tRNA, and (3) an orthogonal ncAA should not be accessible for an aminoacylation reaction with host RS. Satisfaction of all these requirements creates an orthogonal system and ensures successful GCE.

Among the three stop codons in the genetic code, the amber stop codon (UAG) is the most widely used due to its lowest frequency in mRNA transcripts in prokaryotes and eukaryotes. However, 20% of proteins of the mammalian proteome use the amber stop codon for translation termination, and thus, aminoacylated suppressor tRNAs can potentially recognize the UAG site not only in the POI transcript but also in an mRNA encoding housekeeping protein. Such untargeted ncAA incorporation leads to the formation of erroneously long proteins that are mainly uncharacterized and potentially toxic for cells. The construction of designer membraneless organelles – inspired by the concept of phase separation – has addressed this general drawback of GCE in mammalian cells called orthogonally translating (OT) organelles, short OTOs.[5–7] OTOs enable spatial colocalization of the POI mRNA transcript and suppressor tRNA aminoacylation, preferentially directing *in situ* charged suppressor tRNAs to the translation of the desired mRNA (Figure 1B). OTOs thus create a special microenvironment in cells where the desired mRNAs and suppressor tRNAs can be recruited to and maintained for programmed GCE. At the same time, the OTO is still accessible for hundreds of host translational factors to ensure protein translation. Therefore, OTOs feature another type of translation, namely orthogonal translation, where the host translational machinery at the OT organelle site utilizes a second genetic code, in which the UAG codon has the meaning of incorporating a selected ncAA. OTOs preferentially translate the selected amber stop codon-containing mRNA with an expanded genetic code. We thus refer to OTOs as being mRNA- or protein-selective.

OTOs can be assigned to different sites in the cell, e.g. at the plus-end[5] or along microtubules,[7] as well as on the cellular membranes, including plasma membrane (PM), Golgi membrane, endoplasmic reticulum membrane and outer mitochondrial membrane.[6] The latter film-like OT organelles built on the membrane surfaces showed so far the best performance for mRNA-selective GCE realization and were already applied to site-specific labeling and *in situ* studies of protein polymer behavior.[8]

The main goal of GCE technology is to incorporate new functionalities into the proteins, which are delivered to the protein sequence within the applied ncAA. Therefore, the expansion of the ncAA repertoire is highly valuable, and the already existing scope of more than 400 different ncAAs grants an opportunity to exercise many applications, e.g., protein labeling with click chemistry tools,[9,10] development of new antibody-based drugs[11,12] and installation of post-translational modifications into the POI[13,14] (see Refs. [15–17] for reviews and references therein). Transferring this variety of ncAAs to OTOs would equip the synthetic biology toolbox with a new instrument. Previously, only *Methanosarcina mazei* (*Mm*) pyrrolysyl-tRNA synthetase (PylRS) has been used within the OT organelles to realize mRNA-selective GCE for the selected protein[5–7], and thus, only one RS option is currently available for mRNA-selective GCE (Figure 1B and 1C).

In this paper, we tested OT organelles equipped with different RS/tRNA orthogonal pairs commonly exploited for GCE realization in mammalian cells (Figure 1C). To our surprise, we found that mRNA selectivity of OT organelles is easily jeopardized when changing the organelle's orthogonal RS/tRNA pair. We examined various approaches and hypotheses to restore the protein-selective ncAA incorporation of OT organelles, finally leading to an application and optimization of chimeric phenylalanyl-RS/tRNA (chPheRS/chtRNA^{Phe}) pair, which drives site-specific ncAA incorporation with protein selectivity within the OT organelle. The introduction of synthetase mutants into the OT organelle enabled the protein-selective incorporation of new ncAAs, such as 6MeTP (6-methyltryptophan) and 7MeTP (7-methyltryptophan). This study illustrates that the functioning of film-like membraneless OT organelles can be impaired when specific effectors (i.e., RSs) are being changed and demonstrates that much more needs to be studied to thoroughly understand and thus reliably program the functionality of new designer membraneless organelles in mammalian cells.

Results and Discussion

Design of orthogonally translating (OT) organelles

Up to this point, OT organelles were developed as compartments with different shapes (film-like, "blob"-like, and fiber-like) and were built based on a combination of two ways for spatial segregation:

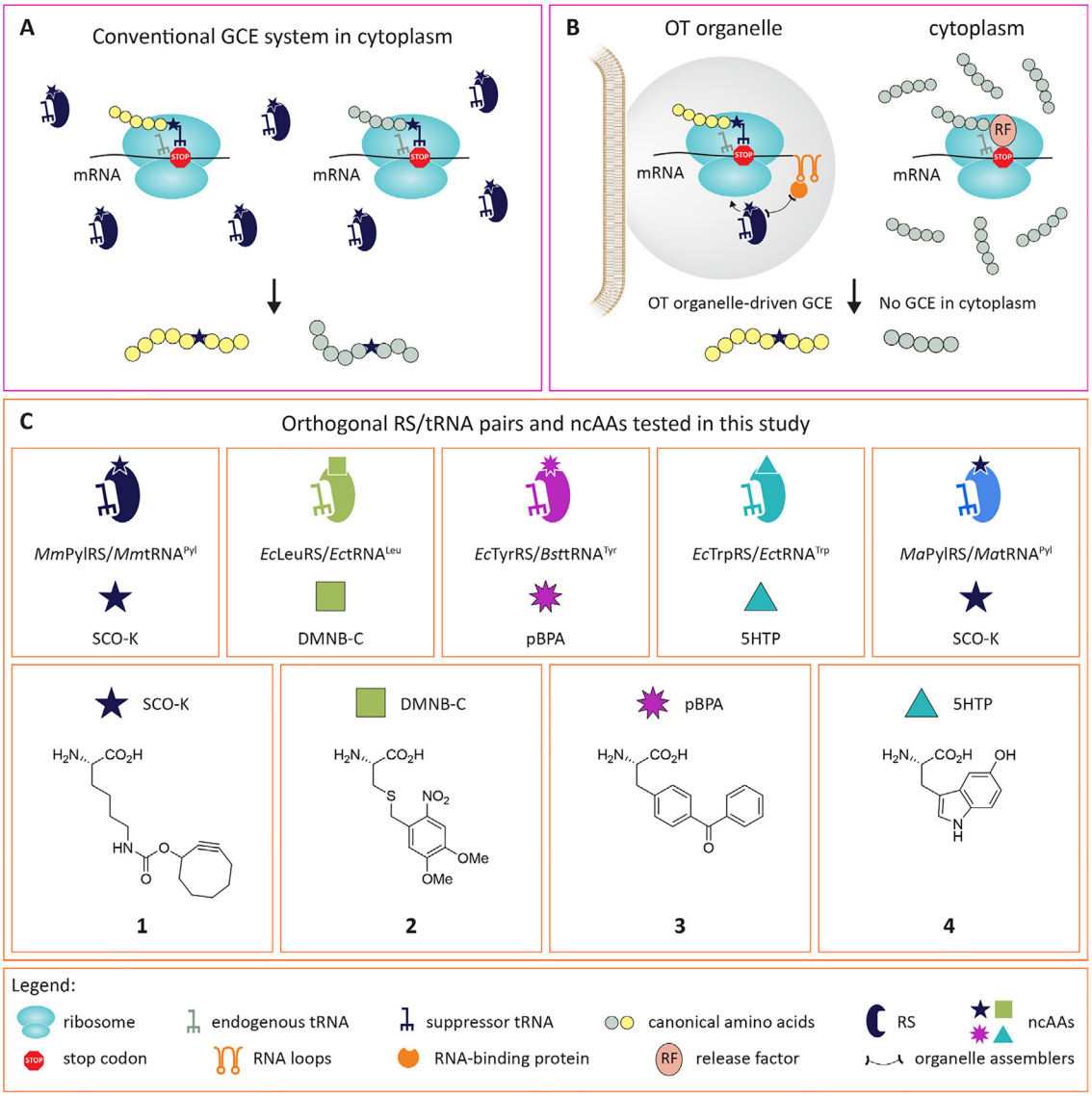

Figure 1. Schematic representation of GCE realized by non-organelle-associated orthogonal pair (**A**) and by orthogonally translating (OT) organelles (**B**). In the non-organelle-associated GCE system, aminoacylated suppressor tRNA can potentially recognize a stop codon in different mRNAs, leading to the non-mRNA- and thus non-protein selective ncAA installation (**A**). OT organelle creates a unique compartment permeable for the host translational machinery and connects tRNA aminoacylation and selected mRNA enrichment at the one cellular localization (**B**). Such strategy allows not only site-specific but also mRNA- and therefore protein-selective ncAA incorporation, which was previously realized using an orthogonal pair of *Methanosarcina mazei* (*M. mazei*) pyrrolysyl-tRNA synthetase and *M. mazei* pyrrolysyl-tRNA. (**C**) Five orthogonal pairs implemented into the plasma membrane-directed OT organelle were tested with complementary ncAAs to determine their capability to incorporate protein-selective ncAA in mammalian cells. *Mm*PylRS denotes *M. mazei* pyrrolysyl-tRNA synthetase, *Mm*tRNA^{Pyl} – *M. mazei* pyrrolysyl-tRNA, *Ec*LeuRS – *Escherichia coli (E. coli)* leucyl-tRNA synthetase, *Ec*tRNA^{Leu} – *E. coli* leucyl-tRNA, *Ec*TyrRS – *E. coli* tyrosyl-tRNA synthetase, *Bst*tRNA^{Tyr} – *Bacillus stearothermophilus* tyrosyl-tRNA, *Ec*TrpRS – *E. coli* tryptophanyl-tRNA synthetase, *Ec*tRNA^{Trp} – *E. coli* tryptophanyl-tRNA, *Ma*PylRS – *Methanomethylophilus alvus* (*M. alvus*) pyrrolysyl-tRNA synthetase, *Ma*tRNA^{Pyl} – *M. alvus* pyrrolysyl-tRNA, SCO-K – N^6-((cyclooct-2-yn-1-yloxy)carbonyl)-L-lysine, **1**, DMNB-C – 4,5-dimethoxy-2-nitrobenzylcysteine, **2**, pBPA – p-benzoyl-L-phenylalanine, **3**, 5HTP – 5-hydroxy-L-tryptophan, **4**.

cellular membrane/cytoskeleton targeting and phase separation.[5–7]

The general design principle seemed that the better the components necessary for the OTO get spatially concentrated, the more mRNA-selective the stop codon suppression worked. To achieve this, proteins were fused to generate a framework of OT organelles:

(i) organelle assemblers, comprised of distinct spatial targeting signals and an intrinsically disordered protein (i.e., fused in sarcoma, FUS), to localize organelles at selected sites of the cell and maintain key players for orthogonal translation highly enriched due to potential phase separation phenomena;
(ii) RNA-binding proteins, which are responsible for recruiting selected mRNAs into the organelle. POI mRNA is modified at 3′UTR with RNA loops that complementarily interact with the RNA-binding protein in the organelle construct. Tight interaction of POI mRNA and RNA-binding protein confers efficient and selective recruitment of selected mRNA to the OT organelle site, e.g., ms2 bacteriophage coat protein (MCP) in the organelle construct recognizes ms2 loops[18] in the 3′UTR of POI mRNA. The MCP is fused to the organelle assembler and provides the POI mRNA enrichment at the organelle;
(iii) RS fused to the organelle assembler (e.g., *Mm*PylRS) to provide local aminoacylation of the suppressor tRNA within the organelle (Figure 1B).

OTOs can be directed to various sites of the cell, e.g., PM-targeting signal from the N-terminal domain of the rodent LCK tyrosine kinase (amino acids 1–10) navigates the organelle to PM to build a film-like PMP organelle (the suffix P denotes the presence of the intrinsic disorder-rich protein FUS which is prone to undergo phase separation at high concentrations). The design of the PMP organelle containing *Mm*PylRS is presented as follows ("–" denotes a genetic fusion):

$LCK_{1–10}$-FUS-MCP-*Mm*PylRS [PMP(*Mm*PylRS)].

Such organelle design enables the fulfillment of two crucial criteria for the proper OT organelle functioning. First, it brings together local suppressor tRNA aminoacylation and enrichment of POI mRNA at the organelle site. Second, such protein framework of the OTO creates a distinct but for the host translational machinery still permeable compartment with a unique microenvironment in the cell. The presented concept of the organelle design was previously successfully employed for the protein-selective ncAA incorporation in mammalian cells[6] and thus was selected for further investigation in this study.

OT organelles equipped with RS/tRNA pairs, different from MmPylRS/$MmtRNA^{Pyl}$, do not enable protein-selective ncAA incorporation

To assess if introducing other orthogonal pairs into the OTO leads to protein-selective incorporation of ncAAs, we first cloned different synthetases from orthogonal pairs commonly applied in mammalian cells into the organelle constructs. *Escherichia coli (Ec)* leucyl-tRNA synthetase (LeuRS),[13,19–21] *Ec* tyrosyl-tRNA synthetase (TyrRS),[22,23] *Ec* tryptophanyl-tRNA synthetase (TrpRS),[24] and *Methanomethylophilus alvus (Ma)*[25,26] PylRS were selected to replace *Mm*PylRS in PMP constructs (Figure 1C), giving rise to the following fusion proteins:

$LCK_{1–10}$-FUS-MCP-*Ec*LeuRS [PMP(*Ec*LeuRS)],
LCK_{1-10}-FUS-MCP-*Ec*TyrRS [PMP(*Ec*TyrRS)],
LCK_{1-10}-FUS-MCP-*Ec*TrpRS [PMP(*Ec*TrpRS)],
LCK_{1-10}-FUS-MCP-*Ma*PylRS [PMP(*Ma*PylRS)].

Suppressor tRNAs – *Ec* leucyl-tRNA ($EctRNA^{Leu}$), *Bacillus stearothermophilus (Bst)* tyrosyl-tRNA ($BsttRNA^{Tyr}$), *Ec* tryptophanyl-tRNA ($EctRNA^{Trp}$), and *Ma* pyrrolysyl-tRNA ($MatRNA^{Pyl}$) – were cloned and employed together with the corresponding RS constructs (Figure 1C). PMP constructs were transiently transfected with matching suppressor tRNAs and the dual-amber reporter GFP^{39TAG}, $mCherry^{189TAG}$-ms2 into HEK293T cells for functional tests of newly assembled OT organelles. OTO performance was analyzed using flow cytometry (FC). GFP and mCherry possess the amber stop codon in the dual-amber reporter, so they only turn fluorescent if the respective stop codon is suppressed. However, only the mRNA of mCherry is tagged with ms2 loops to direct mCherry mRNA to the OT organelle. In the case of protein-selective ncAA incorporation, only mCherry will be fully translated and will be solely identified on an FC plot. If the selective ncAA incorporation does not occur, both proteins will be expressed, resulting in appearance of both mCherry and GFP signals on the FC plot (Figure 2A). To evaluate the protein selectivity of designed OTOs, we quantified the parameter termed "fold change selectivity", defined as the median mCherry signal divided by the median GFP signal of a given system normalized to the respective ratio for the simple non-organelle control of the corresponding RS.

Non-organelle versions of all synthetases provided expression of both mCherry and GFP after the addition of ncAA compatible with the tested orthogonal pairs (N^6-((cyclooct-2-yn-1-yloxy)carbonyl)-L-lysine, SCO-K, **1** was used with *Mm*PylRS/$MmtRNA^{Pyl}$[27] and *Ma*PylRS/$MatRNA^{Pyl}$[26,28] pairs, 4,5-dimethoxy-2-nitrobenzyl cysteine, DMNB-C, **2** – with *Ec*LeuRS/$EctRNA^{Leu}$ pair[20,21]; p-benzoyl-L-phenylalanine, pBPA, **3** – with *Ec*TyrRS/$BsttRNA^{Tyr}$ pair[23]; 5-hydroxy-L-tryptophan, 5HTP, **4** – with *Ec*TrpRS/$EctRNA^{Trp}$ pair[24]; chemical structures of ncAAs are presented in Figure 1C). PMP(*Mm*PylRS) showed 8.5-fold selective expression of mCherry over GFP, consistent with previously published data (Figures 2B, C, and Supplementary Figures 1 and 2). Unexpectedly, none of the other tested orthogonal pairs enabled protein-selective incorporation of added ncAA, demonstrating expression of both mCherry

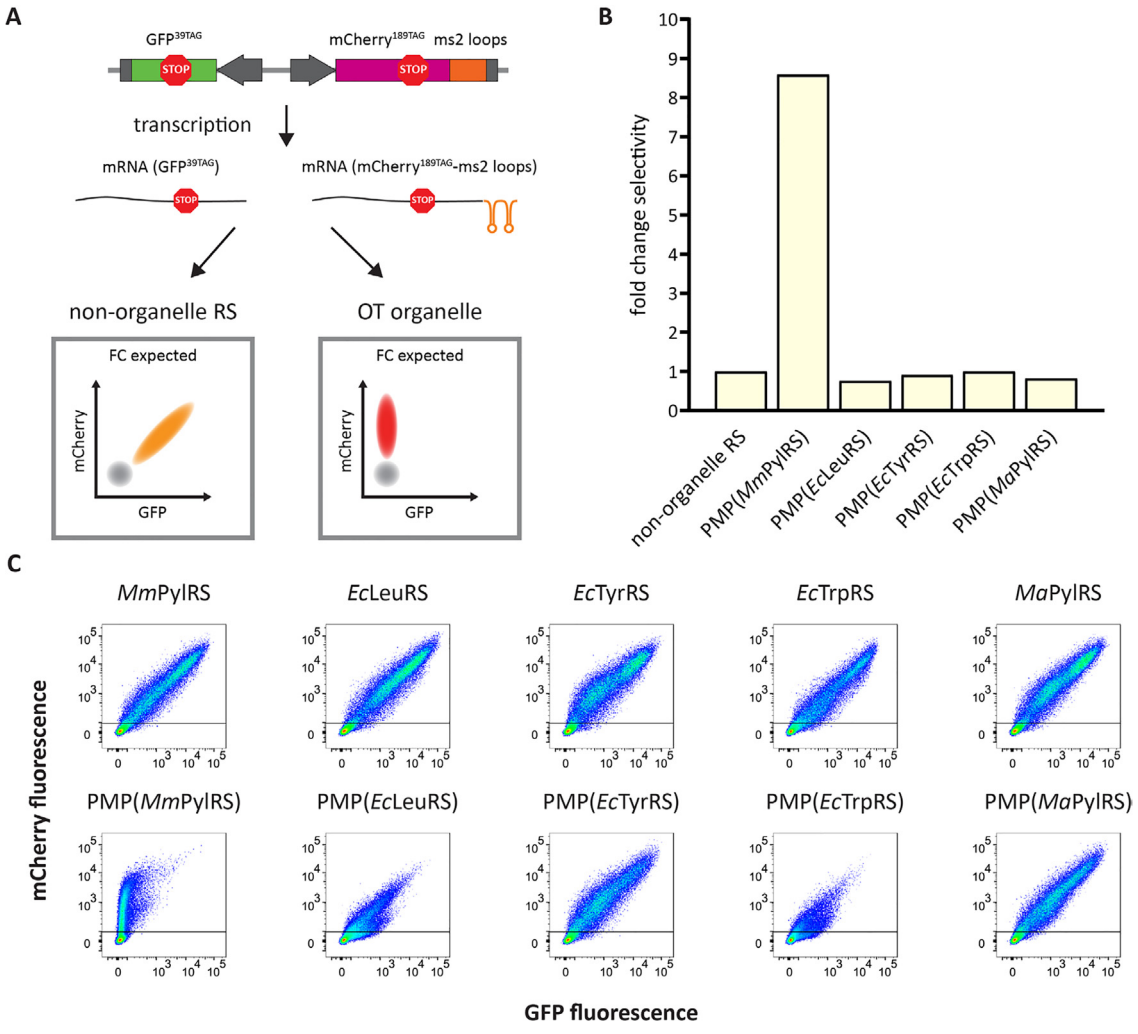

Figure 2. *Mm*PylRS/*Mm*tRNA^{Pyl} is the only orthogonal pair among tested that enables ncAA incorporation in a protein-selective manner when implemented into OTOs. (**A**) The schematic representation of the dual-amber (GFP^{39TAG}, mCherry^{189TAG}-ms2) reporter. In the dual-amber reporter, recruitment of mCherry mRNA, equipped with ms2 loops, to OT organelle is expected to promote mCherry-selective ncAA incorporation, while non-organelle RS, lacking mRNA selection tool, provides GCE and expression for both GFP and mCherry reporters. (**B**) Bar plot illustrating selectivity of OT organelles with different implemented orthogonal pairs. Selectivity is determined in units of fold change selectivity, which is calculated as a ratio of mCherry signal to GFP signal for each organelle normalized to the respective ratio for the corresponding non-organelle-fused RS. (**C**) FC plots show the performance of various non-organelle- and organelle-fused RS while being tested with the dual-amber reporter. FC plots for one performed biological replicate are shown.

and GFP when organelle-fused versions of the synthetases were examined (Figures 2B, C, and Supplementary Figures 1 and 2). These data show that the engineering of new OTOs is not straightforward and pushed us to investigate the reason for the failure of non-functional (meaning non-mRNA-selective) OTOs.

Suppressor tRNAs from different non-working orthogonal pairs do not colocalize well with OT organelles containing the corresponding tRNA synthetase

After failure of new OT organelles to provide ncAA incorporation in a mRNA-selective manner, we checked where PMP organelles with newly implemented synthetases and corresponding suppressor tRNAs are located in the cell. The HEK293T cells were transfected with OT organelle constructs, suppressor tRNA, and NLS (nuclear localization signal)-GFP^{39TAG}-ms2 reporter. The NLS-GFP^{39TAG}-ms2 reporter was used to select for analysis only cells which undergo successful amber suppression (i.e., all plasmids were co-transfected into the selected cell).

Immunofluorescence (IF) labeling was performed to visualize different PMP organelles, and tRNA fluorescence *in situ* hybridization (FISH) was applied for suppressor tRNA staining. For the *Mm*PylRS/*Mm*tRNA^{Pyl} pair, significant

colocalization of PMP organelles and the suppressor tRNA was detected; in cases of all other tested orthogonal pairs, little to no colocalization between PMP organelles and suppressor tRNAs was observed (Figure 3, Supplementary Figures 3 and 4). In most cases, suppressor tRNAs were equally distributed throughout the cell volume, though *Ma*tRNA^{Pyl} was presented almost exclusively in the cytoplasm. This experiment reveals the crucial difference between functional PMP(*Mm*PylRS) organelle and all other non-functional PMP organelles, i.e., the absence of a steep suppressor tRNA gradient in non-selective designer organelles.

Dissociation constants reported for RS/tRNA pairs similar to ones used in this study are available from the literature, and all seem to lie in the range between 0.2 and 2 μM: (i) 0.2 μM for *M. barkeri* PylRS/tRNA^{Pyl}[29] (*Mb*PylRS is a close homolog of *Mm*PylRS from the same *pylSn-pylSc* fusion class of PylRS family), (ii) 0.2 μM for *Ec*LeuRS/*Ec*tRNA^{Leu},[30] (iii) 0.3 μM for *Ec*TyrRS/*Ec*tRNA^{Tyr},[31] and (iv) 2 μM for *Ec*TrpRS/*Ec*tRNA^{Trp}.[32] Noteworthy, dissociation constant values for *E. coli* RS/tRNA pairs were measured using wild type (WT) tRNA with a natural anticodon complementary to the sense codon. However, to perform GCE, *E. coli* suppressor tRNAs with a mutated anticodon to recognize the stop codon in the mRNA are required to direct ncAA incorporation at the programmed site, and thus, we can expect the dissociation constants to be equal or lower than reported for the wild type tRNAs. In this study, we used

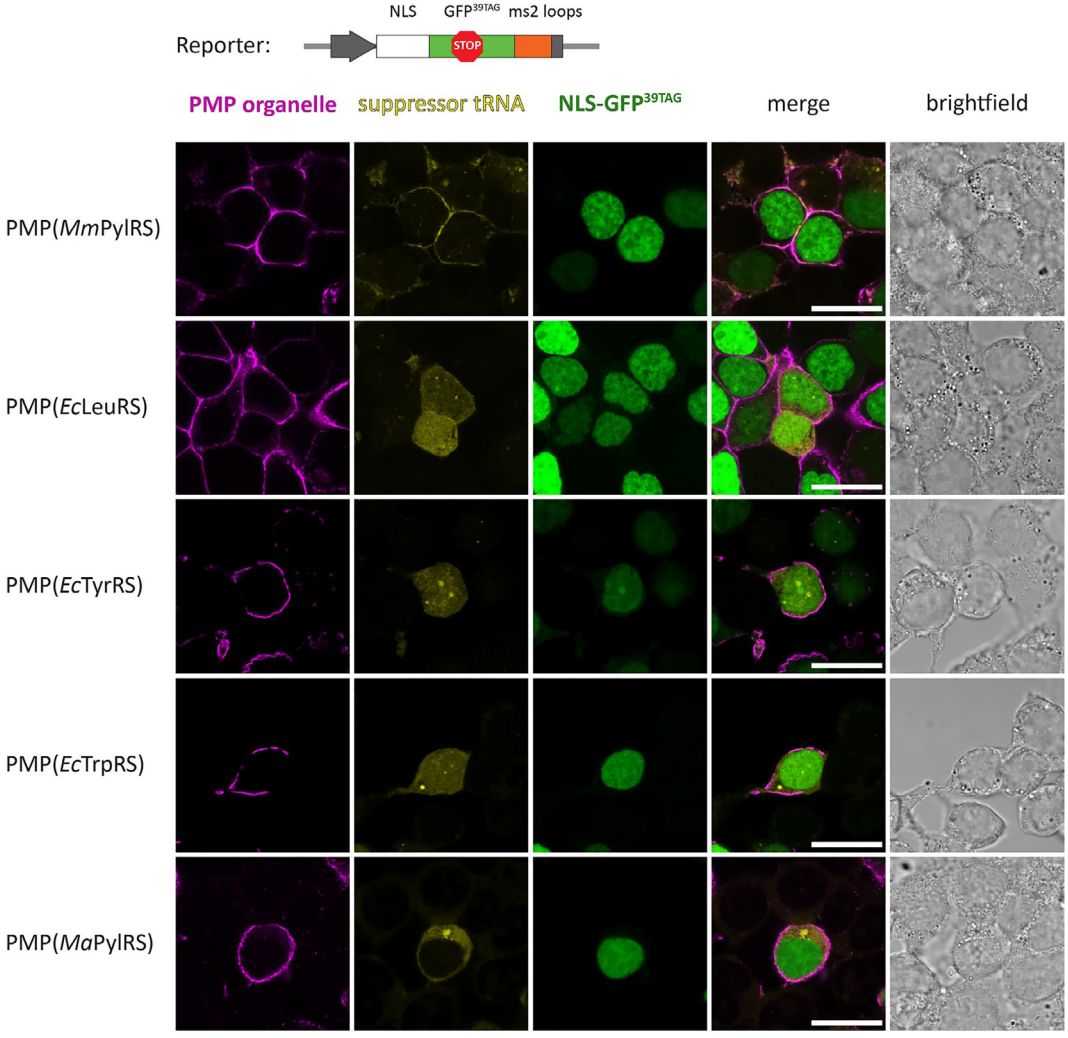

Figure 3. Immunofluorescence and tRNA FISH demonstrate the colocalization between a designer organelle and suppressor tRNA only for the *Mm*PylRS/*Mm*tRNA^{Pyl} pair. Designer organelles were visualized using secondary antibodies conjugated with Cy3 (magenta). Suppressor tRNAs were labeled using tRNA FISH with specially designed Cy5-conjugated probes, which specifically bind to the studied suppressor tRNA (yellow). The NLS-GFP^{39TAG}-ms2 reporter was applied to identify cells with successful GCE realization (green). Scale bars: 20 μm.

E. coli suppressor tRNAs with CUA anticodon to install the ncAA at the introduced amber stop codon site. Because some of the RSs (e.g., *Ec*TyrRS and *Ec*TrpRS) also recognize the anticodon region, the exact dissociation constants for the GCE-performing mutant RS/tRNA pairs are not readily available. Introduced mutations in the anticodon of *E. coli* suppressor tRNAs might potentially lead to a change in the dissociation constant and to weaker binding of the suppressor tRNAs to cognate RSs. Another important parameter for the characterization of RSs is the aminoacylation rate (k_{cat}). Interestingly, *Mm*PylRS was reported to charge its suppressor tRNA much slower (0.002–0.008 s^{-1})[33,34] compared with *E.coli* RSs, which have aminoacylation rates around 1000-fold higher: (i) 6 s^{-1} for *Ec*LeuRS,[30] (ii) 0.7–11 s^{-1} for *Ec*TyrRS,[31,35] and (iii) 13–44 s^{-1} for *Ec*TrpRS[32,36] (all reported for natural *E. coli* tRNAs charged with canonical AAs). Based on this, one hypothesis to explain a failure of non-functional orthogonal pairs could be that aminoacylation of *E. coli* suppressor tRNAs happens too fast at the OT organelle site such that the host translational machinery is not able to consume all charged tRNAs for orthogonal translation, allowing charged tRNAs to drift away from the OT organelle and leading to non-protein-selective ncAA installation. However, *Ma*PylRS, another archeal RS from the *ΔpylSn* class of PylRS family, demonstrated a similar aminoacylation rate (0.005 s^{-1})[37] as *Mm*PylRS and still did not enable protein-selective ncAA incorporation in our tests with OT organelles. It is possible that further kinetic studies could provide a clue as to the failure of the particular orthogonal RS/tRNA pair to provide protein-selective GCE while being implemented into the OT organelle. However, we pursued a different route to provide a path towards adding more RS/tRNA to OTOs.

Reengineering approaches to restore mRNA selectivity for non-functional designer organelles

To recover the mRNA selectivity for non-functional OT organelle, we developed several strategies, including (1) suppressor tRNA titration, (2) ncAA titration, (3) addition of NES (nuclear export signal) into the organelle construct, (4) implementation of multiple RS copies into the organelle protein fusion, and (5) introduction of RNA loop into the V-arm of the suppressor tRNA, and tested them for OTOs equipped with *Ma*PylRS/*Mat*RNA^{Pyl} pair (Figure 4). Below, we describe these strategies in detail.

Structural differences in MmPylRS/MmtRNA^{Pyl} and MaPylRS/MatRNA^{Pyl} orthogonal pairs. To solve the problem of non-protein-selective ncAA incorporation in non-functional designer organelles, we focused our attempt on PMP (the organelle with the best spatial separation from the cytoplasm) combined with the *M. alvus* PylRS system. However, despite *Ma*PylRS/*Mat*RNA^{Pyl} pair being a close relative to the working *Mm*PylRS/*Mm*tRNA^{Pyl} pair, we did not observe any protein-selective functionality of the OTO (Figure 2B and 2C).

*Mm*PylRS belongs to the *pylSn-pylSc* fusion class of the PylRS family, and the *Mm*PylRS structure includes two domains: i) an N-terminal domain (NTD) that interacts with nucleotides residing in the variable loop (V-loop) and T-arm of *Mm*tRNA^{Pyl}, and thus NTD *Mm*PylRS is believed to be responsible for *Mm*tRNA^{Pyl} recognition and ii) a C-terminal domain (CTD), which is a catalytic domain and performs *Mm*tRNA^{Pyl} aminoacylation[38] (Figure 5A, left part, and Supplementary Figure 5). Alongside, *Ma*PylRS represents the *ΔpylSn* class of the PylRS family, does not have an NTD, and is homologous to the CTD of *Mm*PylRS[25,26] (Figure 5A, middle part, and Supplementary Figure 5).

Alignment of CTD *Mm*PylRS and *Ma*PylRS, as well as further comparison of crystal structures, revealed that binding pockets of the enzymes are structurally similar and mutations directed towards the incorporation of particular ncAA can be transferred from *Mm*PylRS to *Ma*PylRS.[26,28] Interestingly, despite lacking a specialized tRNA-binding domain, *Ma*PylRS demonstrated higher yields for installing some ncAAs,[39] demonstrating the potential for GCE applications.

Sequences of *Mm*tRNA^{Pyl} and *Mat*RNA^{Pyl} have numerous differences distributed in the acceptor stem, D-stem-loop, anticodon stem, and T-stem-

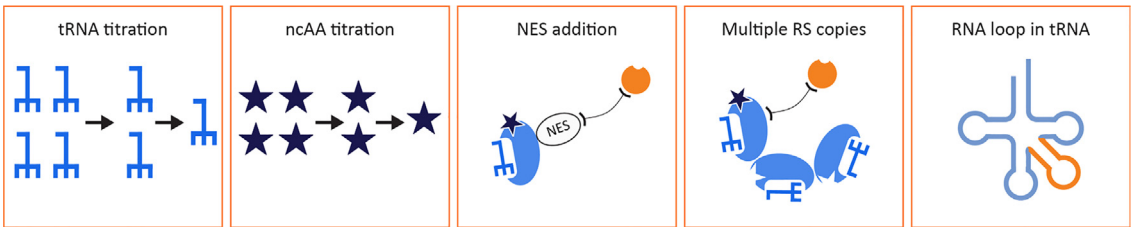

Figure 4. Different tested strategies for repair of the functionality of the PMP organelle equipped with *Ma*PylRS/*Mat*RNA^{Pyl}. Legend is the same as in Figure 1. See details for each strategy in the text.

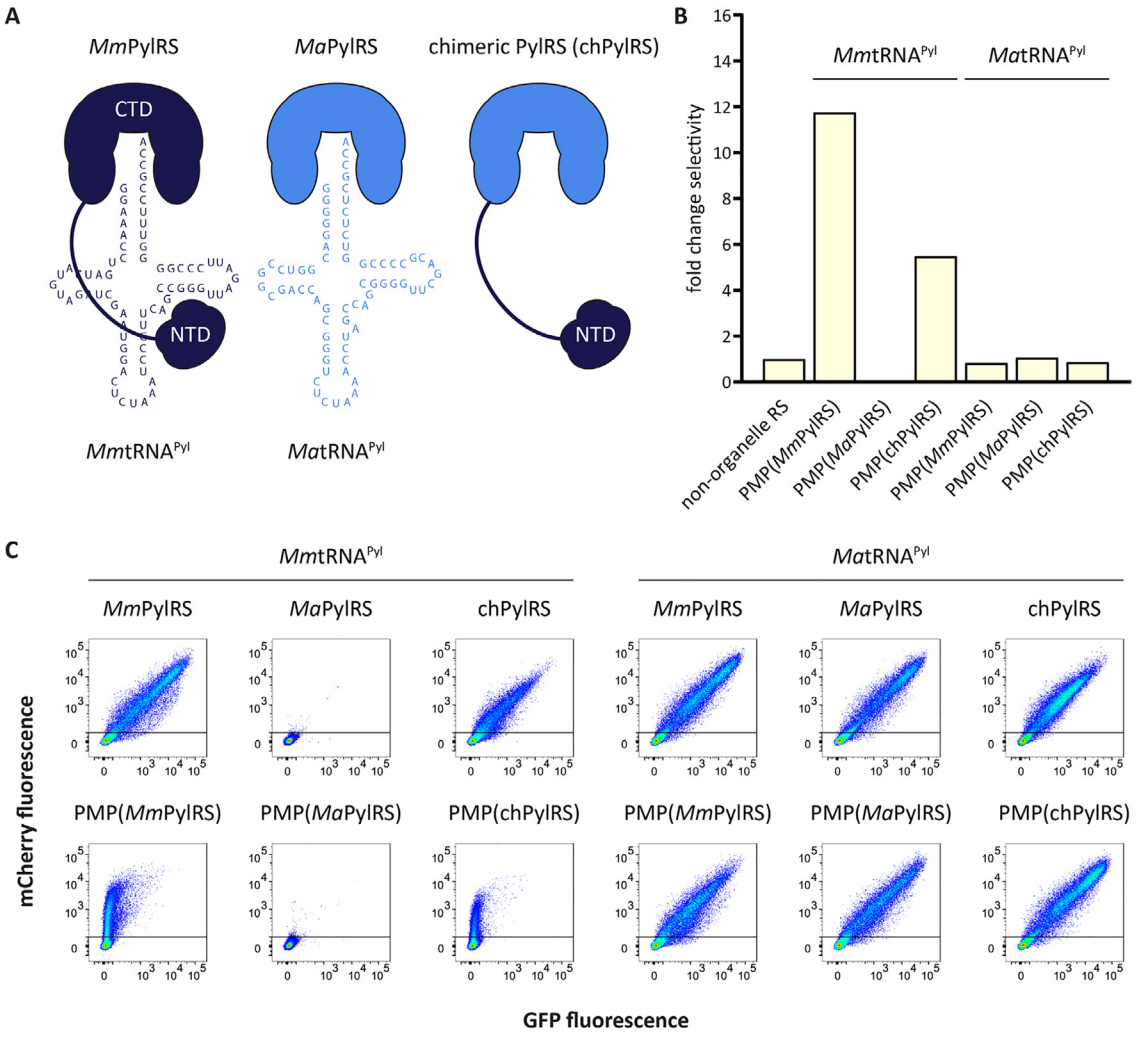

Figure 5. PMP(chPylRS) provides protein-selective ncAA installation when used together with *Mm*tRNA^{Pyl}. (**A**) The schematic representation of the PylRS (*Mm*PylRS, *Ma*PylRS, and chPylRS) and suppressor tRNA^{Pyl} (*Mm*tRNA^{Pyl} and *Mat*RNA^{Pyl}) structures. (**B**) Bar plot illustrating selectivity of OT organelles with different implemented PylRS orthogonal pairs. Selectivity is determined in units of fold change selectivity, calculated the same way as in Figure 2. (**C**) FC plots show the performance of various non-organelle- and organelle-fused PylRSs while being tested with the dual-amber reporter. FC plots for one performed biological replicate are shown.

loop (Figure 5A). Comparison of *Mm*tRNA^{Pyl} with *Mat*RNA^{Pyl} reveals two distinguishing structural features: (i) a shorter 4-nt D-loop in the *Mat*RNA^{Pyl} structure and (ii) an unpaired A38 in the anticodon stem of *Mat*RNA^{Pyl}.[25,26] Despite the differences in the tRNA sequences, *Mm*PylRS can cross-recognize and aminoacylate *Mat*RNA^{Pyl}, while *Ma*PylRS does not enable GCE when used together with *Mm*tRNA^{Pyl}.[25,26] This monodirectional orthogonality between *Mm* and *Ma* pairs was fixed by the evolution of the *Mat*RNA^{Pyl} V-loop to make it non-recognizable for *Mm*PylRS, therefore creating two mutually orthogonal pairs in mammalian cells.[25,26] Considering the likeness of *Mm* and *Ma* orthogonal pairs and the potential of using *Ma*PylRS/*Mat*RNA^{Pyl} pair within the OTO, we examined several strategies (Figure 4) in an attempt to restore the protein-selective ncAA incorporation realized by a designer organelle equipped with the *Ma* pair.

Substrate (ncAA or suppressor tRNA) titration does not correct the function of OT organelles equipped with MaPylRS. First, we tried to titrate down the amount of transfected suppressor *Mat*RNA^{Pyl} or concentration of SCO-K in the medium to obtain mRNA selectivity for PMP (*Ma*PylRS) (Figure 4). The idea was to decrease the aminoacylation level of suppressor tRNAs, which takes place at the OT organelle site and find a “sweet spot” where all charged suppressor tRNAs can be exploited for orthogonal translation at the organelle. Different amounts of transfected *Mat*RNA^{Pyl} plasmid (from 300 ng down to 1 ng)

and various concentrations of SCO-K (from 250 μM to 0.24 μM) were tested together with PMP (*Ma*PylRS) organelle and the dual-amber reporter. However, such trials did not restore any shift towards mCherry-selective ncAA incorporation (Supplementary Figures 6 and 7).

Adding a nuclear export signal (NES) and inserting multiple MaPylRS copies to the OT organelle does not recover protein-selective ncAA incorporation. In the seminal design of the OT organelle, NES-PylRS^{AF} was fused to the PM-directing organelle assemblers to create PMP(*Mm*PylRS). The addition of NES to the N-terminal part of *Mm*PylRS was previously demonstrated to enhance GCE efficiency in mammalian cells,[40] and thus, this upgraded version of the synthetase was selected for integration into the OT organelle. We equipped *Ma*PylRS with NES and integrated this construct into the PMP organelle (giving rise to PMP(NES-*Ma*PylRS) organelle) to test if the addition of NES provides any change and helps to recover the correct organelle functionality (Figure 4). PMP(NES-*Ma*PylRS) application did not reveal any improvement for protein-selective ncAA incorporation (Supplementary Figure 8). Another approach for restoration of protein selectivity for the OT organelle with the introduced *Ma* pair implies the increase of binding sites for suppressor tRNAs in the organelle to halt them at the organelle site and direct them towards orthogonal organelle translation (Figure 4). Fusion organelle constructs with two and three copies of *Ma*PylRS were designed to equip the designer organelle with a bigger capacity for *Mat*RNA^{Pyl} binding and tested with *Mat*RNA^{Pyl} and the dual-amber reporter. Unfortunately, introducing PMP organelles with multiple copies of *Ma*PylRS did not allow protein-selective ncAA incorporation (Supplementary Figure 9).

Introducing protein-binding RNA loops into V-loop of suppressor tRNAs to repair OT organelle function. Since diffuse tRNA localization in the cell but outside the OT organelle was detected in the FISH experiment and thus disturb the protein-selective function of the organelle, we considered another concept involving active recruitment of suppressor tRNAs into the organelle where they can be further employed for aminoacylation. Protein-RNA interaction can be used to actively target RNA to the organelle site in the same way as we applied ms2 RNA loops at the 3′UTR of mCherry mRNA to direct the mRNA to the organelle. tRNAs are rigid clover-leaf structures in which insertion of another loop into structurally important tRNA parts can destabilize tRNAs and cause them to lose their function. However, V-loop of tRNAs appears to be the best place for tRNA engineering since it does not crucially contribute to the stability of tRNA structure (Figure 4).

To test the concept, ms2 and boxB[41,42] RNA loops were inserted into the V-loop of *Mat*RNA^{Pyl} to generate eight different *Mat*RNA^{Pyl} variants (see Supplementary Figure 10 for the tRNA designs). The modified tRNAs were first examined with the simple non-organelle version of *Ma*PylRS and iRFP-GFP^{39TAG} reporter to check if such newly constructed tRNAs are stable and can efficiently work with the *Ma*PylRS and host translational machinery to realize GCE. The iRFP-GFP^{39TAG} reporter contains iRFP as a transfection control and GFP^{39TAG}, which can only be expressed in the presence of RS/tRNA orthogonal pair and after ncAA addition. No GFP and thus no GCE signal was obtained in the case of using modified *Mat*RNA^{Pyl} variants (Supplementary Figure 11), pointing to a potential problem with tRNA stability and/or with the functionality of the modified tRNAs with the *Ma*PylRS or other translational components.

Natural *Mat*RNA^{Pyl} has only three nucleotides in the V-loop, and the insertion of RNA loops represents a big change in the sequence and structure of the tRNA, imaginably leading to the problems described above. We then decided to check if modification of the V-loop with RNA loops helps protein-selective ncAA incorporation realized by RS/tRNA pair, where suppressor tRNA has an intrinsically bigger V-loop in the tRNA structure. We selected the *Ec*LeuRS/*Ec*tRNA^{Leu} pair since *Ec*tRNA^{Leu} has 14 nucleotides in its V-loop, and it was previously demonstrated that the nucleotide sequence can be changed within this tRNA region while obtaining still functionally active *Ec*tRNA^{Leu}.[43] Thirteen *Ec*tRNA^{Leu} variants were generated by replacing the natural V-loop sequence of the tRNA with ms2, pp7[44,45], or boxB loop (see Supplementary Figure 12 for the tRNA designs) and examined with the non-organelle version of *Ec*LeuRS and the iRFP-GFP^{39TAG} reporter. Gratifyingly, modified *Ec*tRNA^{Leu} variants enabled GCE realization in mammalian cells. Moreover, the *Ec*tRNA^{Leu}-13 variant was operating at the same level of GCE efficiency as suppressor *Ec*tRNA^{Leu} WT (Supplementary Figures 13–15). We also tested if the RNA loop embedded into the tRNA structure can still interact with the partner RNA-binding protein and measured GCE efficiency for the modified tRNAs in the presence of MCP, PCP, and λN22 proteins, which bind to ms2, pp7, and boxB RNA loops, respectively. If the protein-tRNA interaction occurs, the GCE efficiency of samples with additionally introduced RNA-binding proteins is expected to be lower. Such a drop in GCE efficiency can be observed due to the functional protein-tRNA interaction, which potentially blocks the accessibility of modified tRNA for the orthogonal synthetase and thus decreases the tRNA aminoacylation rate. Indeed, for many of our modified *Ec*tRNA^{Leu} variants, we observed diminished GCE efficiency in the presence of RNA-binding proteins

(Supplementary Figures 13 and 14), indicating that RNA loops inside tRNA structure are available for protein-tRNA interactions. These data confirm that some suppressor tRNAs can potentially be modified at the site of V-loop, maintain GCE activity, and interact with paired RNA-binding proteins; thus, our results are consistent with the previously reported findings.[46] After these successful tests, we applied the best-performing *Ec*tRNA^{Leu}-13 variant for experiments with PMP(*Ec*LeuRS) and LCK$_{1-10}$-EWSR1-4xλN22 construct to check if the newly designed suppressor tRNA solves the challenge of protein-selective OT organelle-driven ncAA incorporation. The LCK$_{1-10}$-EWSR1-4xλN22 construct is required for tRNA recruitment to the organelle, contains intrinsically disordered protein EWSR1 (Ewing sarcoma breakpoint region 1), and was previously successfully used with film-like OT organelles.[6] However, the simultaneous use of PMP(*Ec*LeuRS), LCK$_{1-10}$-EWSR1-4xλN22 and *Ec*tRNA^{Leu}-13 did not yield a mCherry-only population in the test with the dual-amber reporter (Supplementary Figure 16) and therefore did not allow to achieve ncAA incorporation in a protein-selective manner in OTOs.

Optimized chimeric PheRS/tRNA pair provides protein-selective ncAA incorporation within the OT organelles

After obtaining unsuccessful results using the described strategies, we decided to use a conceptually distinct approach to solve the selectivity challenge for OT organelles. Recruitment and maintenance of suppressor tRNAs at the OT organelle site appear critical to a functional OT organelle. In the case of *Mm*PylRS, the NTD might provide the additional level of interaction with the *Mm*tRNA^{Pyl} compared with *Ma*PylRS/*Ma*tRNA^{Pyl} pair and thus can keep the *Mm*tRNA^{Pyl} at the organelle aminoacylation machinery and enable organelle-driven orthogonal translation. Given the high similarity between the V-loop and T-stem regions of *Mm*tRNA^{Pyl} and *Ma*tRNA^{Pyl}, we tested whether the addition of NTD *Mm*PylRS to *Ma*PylRS would enhance the interaction between *Ma*PylRS and *Ma*tRNA^{Pyl}, thereby restoring protein-selective ncAA incorporation in the OT organelles. This PylRS construct was called chimeric PylRS (chPylRS, Figure 5A; see Supplementary Figure 5 for the detailed synthetase design).

We first checked with the dual-amber reporter whether the newly designed chPylRS is active and can perform GCE in cooperation with *Mm*tRNA^{Pyl} or *Ma*tRNA^{Pyl} and observed successful GCE realization in the presence of each of two suppressor tRNAs (Figures 5B, 5C, and Supplementary Figure 17). A positive result for a pair of chPylRS and *Mm*tRNA^{Pyl} hints at tighter interaction between NTD-equipped *Ma*PylRS and *Mm*tRNA^{Pyl}, which starts enabling successful GCE performance, while the previously non-modified version of *Ma*PylRS did not react with *Mm*tRNA^{Pyl} (Figures 5B, C, and Supplementary Figure 17). Next, we implemented chPylRS into the PMP organelle construct and examined a newly created PMP(chPylRS) in parallel with PMP(*Mm*PylRS) and PMP(*Ma*PylRS) for protein-selective ncAA incorporation in the presence of *Mm*tRNA^{Pyl} or *Ma*tRNA^{Pyl}. Rewardingly, use of PMP(chPylRS) with *Mm*tRNA^{Pyl} allowed a 5.4-fold selectivity towards mCherry expression over GFP expression (Figures 5B, C, and Supplementary Figures 17 and 18). Interestingly, neither well-established PMP(*Mm*PylRS) nor newly developed PMP(chPylRS) provided orthogonal translation when the PMP organelles were applied together with *Ma*tRNA^{Pyl}. This observation demonstrates the significance of the NTD *Mm*PylRS and *Mm*tRNA^{Pyl} interaction for successful protein-selective ncAA incorporation facilitated by OT organelles.

Inspired by these results, we studied another previously published orthogonal RS with a domain architecture similar to chPylRS – chimeric human mitochondrial (*Hmt*) PheRS or chPheRS[47]). Here, chPheRS is made of: (1) an NTD *M. barkeri* PylRS (close homolog of *Mm*PylRS, residues 1–149 with IPYE mutations,[48] (2) a part of CTD *Mm*PylRS sequence (residues 185–240), and (3) a catalytic domain from human *Hmt*PheRS (residues 29–359, Figure 6A). ChPheRS works in tandem with a chimeric phenylalanyl-tRNA (chtRNA^{Phe}) comprised of (1) acceptor stem from human cytosolic tRNA^{Phe} (with mutations A6G, U66C[49] and (2) rest tRNA backbone from *Mm*tRNA^{Pyl} (with mutation U25C, Figure 6A). This orthogonal chPheRS/chtRNA^{Phe} pair enabled successful GCE realization both in prokaryotes and eukaryotes in presence of various ncAAs, e.g., phenylalanine derivatives.[47] We first started experiments with the reported sequence of chPheRS-1, which bears mutations T467G and A507G allowing p-azidophenylalanine (pAzF, **5**) incorporation; we called this version of the synthetase chPheRS-1v0. A new PMP organelle was constructed to contain chPheRS-1v0, and the newly formed PMP(chPheRS-1v0) was examined together with the chtRNA^{Phe} and the dual-amber reporter for the capability of protein-selective ncAA incorporation. The samples were incubated with 2 mM pAzF as a ncAA. Satisfyingly, use of PMP(chPheRS-1v0) provided a 1.5-fold increase in mCherry over GFP signal (Figure 6B, C, and Supplementary Figures 19 and 20).

We then investigated if optimizing the chPheRS sequence can enhance the system's selectivity and designed two new design variants of chPheRS, namely chPheRSv1 and chPheRSv2. The new versions of chPheRS contain: (1) NES fused to the N-terminal part of the synthetase, (2) *Mm*PylRS sequence with various lengths

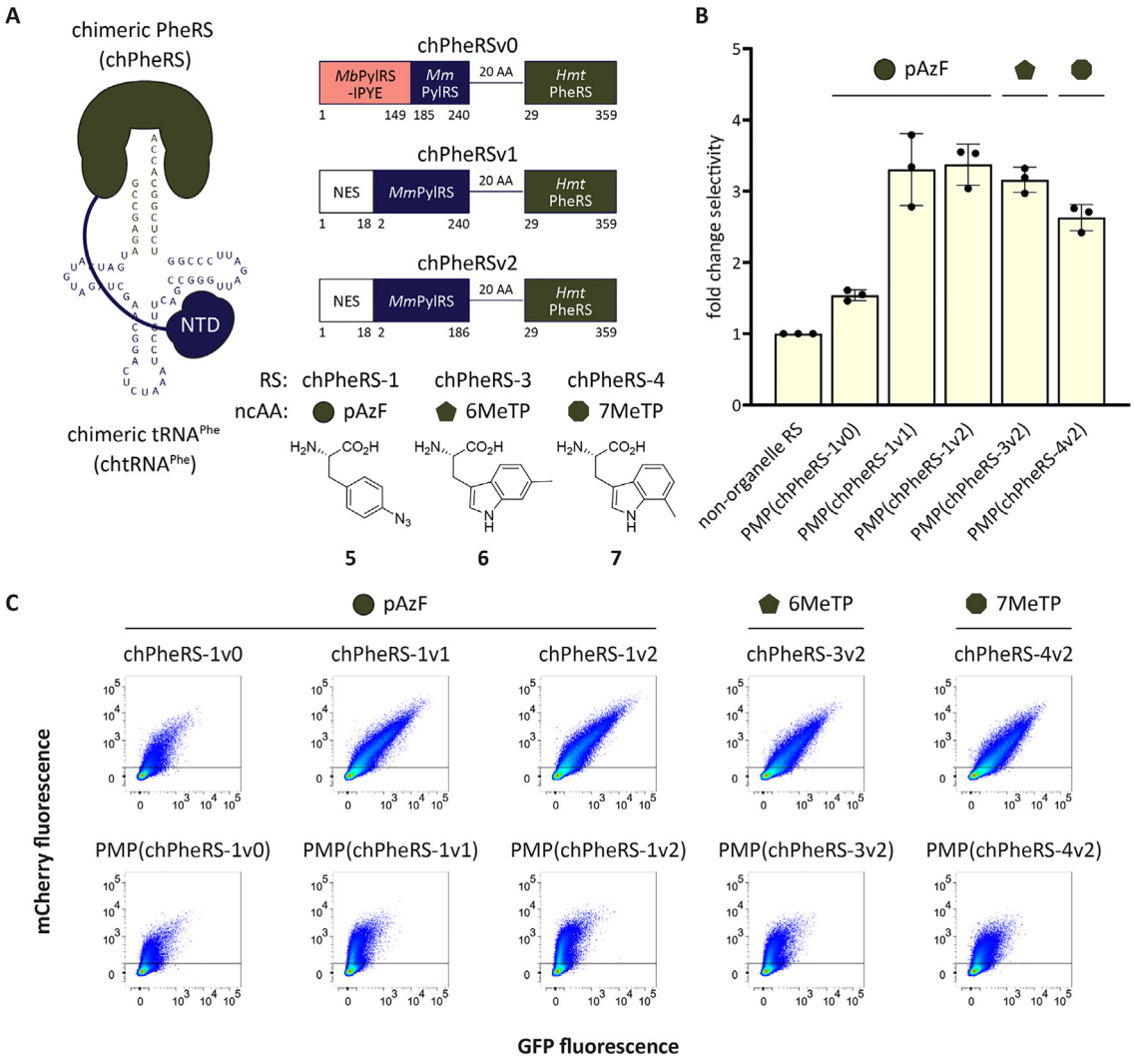

Figure 6. PMP(chPheRS) organelles enable protein-selective incorporation of different ncAAs. (**A**) The schematic representation of the chPylRS structure and enzyme designs, chtRNA^{Phe}, and ncAA chemical structures (pAzF - p-azidophenylalanine, **5,** 6MeTP - 6-methyltryptophan, **6,** 7MeTP - 7-methyltryptophan, **7**). (**B**) Bar plot illustrating selectivity of OT organelles with different implemented chPheRS/chtRNA^{Phe} orthogonal pairs in the presence of three different ncAAs (pAzF, **5**; 6MeTP, **6**; 7MeTP, **7**). Selectivity is determined in units of fold change selectivity, calculated the same way as in Figure 2. Bars show the mean of fold change selectivity values from three independent experiments; error bars represent standard deviation. (**C**) FC plots show the performance of various non-organelle- and organelle-fused chPheRSs while being tested with the dual-amber reporter in the presence of three different ncAAs (pAzF, **5**; 6MeTP, **6**; 7MeTP, **7**). Concatenated data from three independent experiments are shown.

(residues 2–240 for chPheRSv1 and residues 2–186, same as in chPylRS, for chPheRSv2), and (3) the catalytic domain from human *Hmt*PheRS (Figure 6A). We then tested new organelles PMP (chPheRS-1v1) and PMP(chPheRS-1v2) and could achieve a 3.3-fold increase of pAzF incorporation into mCherry over GFP while using PMP(chPheRS-1v2) (Figures 6B, C, and Supplementary Figures 19 and 20). The selective incorporation of pAzF in place of canonical amino acids into the reporter protein, facilitated by organelles with chimeric synthetases, was confirmed through mass spectrometry (see Supplementary Figures 21–23). Notably, non-organelle variants chPheRS-1v1 and chPheRS-1v2 outperformed initial non-organelle-fused chPheRS-1v0 in GCE efficiency, demonstrating up to a 2.6-fold (using chPheRS-1v1) and up to a 2.2-fold (using chPheRS-1v2) GCE enhancement for GFP and mCherry, respectively, compared with chPheRS-1v0 (Supplementary Figure 24). This data indicates that optimization of the N-terminal part of chimeric PylRS-based synthetases can serve as an efficient strategy for enhancing GCE performed by chimeric orthogonal pairs alongside with evolution of C-terminal part of

the chimeric synthetase and tRNA evolution.[50] ChPheRS was also previously shown to incorporate several tryptophan derivatives, e.g., 6-methyltryptophan (6MeTP, **6,** Figure 6A) and 7-methyltryptophan (7MeTP, **7,** Figure 6A),[47] which, to our knowledge, have not been reported as substrates for PylRS. We used reported sequences ChPheRS-3 (with mutations E391D, T467G, and A507G for 6MeTP incorporation) and ChPheRS-4 (with mutations F464V, T467G, and A507G for 7MeTP incorporation)[47] to build new organelles and tested PMP(chPheRS-3v2) and PMP (chPheRS-4v2) with the suppressor chtRNA^{Phe} and the dual-amber reporter. We obtained a 3.1-fold and a 2.6-fold increase in selectivity for 6MeTP and 7MeTP incorporation, respectively (Figures 6B, C, and Supplementary Figures 20 and 25), thus extending the ncAA toolbox of OT organelles with tryptophan analogs. Also for PMP(chPheRS-3v2) and PMP(chPheRS-4v2) organelles, the incorporation of 6MeTP or 7MeTP, respectively, was verified through mass spectrometry (see Supplementary Figures 26–29). The experiments with chPheRS confirm the importance of interaction between NTD *Mm*PylRS and *Mm*tRNA^{Pyl} for the correct organelle functionality and, meanwhile, also show that it is possible to integrate other synthetases (e.g., in the form of catalytic domains) into the OT organelle for incorporation of new ncAAs in a protein-selective manner.

In this work, we started out by testing whether different orthogonal RS/tRNA pairs – widely used for GCE – could be used to engineer novel designer OTOs in mammalian cells. Despite the modular design of OTOs, none of the existing RS/tRNA pairs besides the *Mm*PylRS/*Mm*tRNA^{Pyl} system enabled protein/mRNA-selective engineering. We developed several design strategies to address this limitation to restore the mRNA selectivity as observed for the OTOs equipped with the *Ma*PylRS/*Ma*tRNA^{Pyl} pair. We demonstrated that the concept of a chimeric synthetase allowed to determine key players for proper organelle functionality and guided further organelle development. This concept was further applied to create new mRNA-selective OTOs employing the rationally optimized chPheRS/chtRNA^{Phe} pair. These new OTOs expanded the ncAA toolbox by enabling the mRNA-selective incorporation of tryptophan derivatives and suggested that other RSs (or at least their catalytic domains) could potentially be integrated into our organelle design while maintaining correct OTO functionality. For the chPheRS/chtRNA^{Phe} system, the selectivity gain comes at the cost of efficiency, which has been observed before in OTOs. Thus, OTOs have a particular strength in applications where background reduction is more crucial than absolute production yield, as it is often the requirement in cell biological studies versus those where purification is the ultimate goal. However, further OTO development such as synthetase evolution, promotor tuning, and mRNA stability tuning can be explored to enhance yield.[51–53]

Designer organelles aim to generate unique places in the cell for controlled reactions in a unique biochemical environment that minimizes interactions with the host cell. Understanding enzymology, not just within the cell but even within these particular protein- and RNA-rich environments, is a challenge that needs to be addressed to enable reliable programming of designer synthetic organelles for their foreseeable performance in mammalian cells. Our study reveals crucial conditions for the correct functionality of OTO when expanding the genetic code with different RS/tRNA pairs and provides a new path to encode new ncAAs via designed OTO-compatible chimeric RS/tRNA pairs.

Materials and Methods

Cell culture

HEK293T cells (ATCC, CRL-3216) were cultured in Dulbecco's modified Eagle's medium (DMEM, Gibco, 41965-039) supplemented with 10% FBS (Sigma–Aldrich, F7524), 1% penicillin–streptomycin (Sigma–Aldrich, P0781), 1% L-glutamine (Sigma–Aldrich, G7513), and 1% sodium pyruvate (Life Technologies, 11360) at 37 °C and 5% CO_2. Cells were passaged every 2–3 days up to 17 passages. For flow cytometry experiments, the HEK293T cells were seeded 20 h prior to transient transfections in 24-well plates (Sarstedt, 83.3922) at a density of 220,000 cells/mL (500 μL/well). For immunofluorescence labeling coupled with tRNA FISH, the HEK293T cells were seeded 20 h prior to transient transfections in 4-well cell imaging cover glasses (Eppendorf) at a density of 220,000 cells/mL (700 μL/well). For mass spectrometry measurements, HEK293T cells were seeded 20 h prior to transient transfections in 100 mm round cell culture dishes (CELLSTAR, Greiner Bio-One) at a density of 220,000 cells/mL (10 mL/dish).

Constructs and cloning

Supplementary Table 1 summarizes the plasmids used in this study.

DNA sequences of *Ec*LeuRS and *Ec*TyrRS were acquired with plasmids, which were a kind gift from the Peter Schultz group (The Scripps Research Institute, La Jolla, USA). *Ec*TrpRS, *Ma*PylRS, and chPheRS-1v0 were obtained by gene synthesis (Genewiz). The synthetase sequences were amplified out of the template plasmids and cloned into a pcDNA3.1 backbone. *Ec*tRNA^{Leu} (*Ec*tRNA^{Leu} WT) and *Bst*tRNA^{Tyr} sequences were ordered as gene synthesis (Mr. Gene). *Ec*tRNA^{Trp},

*Ma*tRNA^{Pyl} (*Ma*tRNA^{Pyl} WT), modified *Ma*tRNA^{Pyl} (*Ma*tRNA^{Pyl}-1-*Ma*tRNA^{Pyl}-8), and chtRNA^{Phe} were inserted into a pUC57 vector via primer annealing cloning method followed by restriction cloning. Modified *Ec*tRNA^{Leu} (*Ec*tRNA^{Leu}-1-*Ec*tRNA^{Leu}-13) were introduced into the pUC57 backbone performing overlap extension PCR followed by Gibson assembly. ChPylRS plasmid was cloned into the pcDNA3.1 via Gibson assembly, fusing *Mm*PylRS and *Ma*PylRS (see Supplementary Figure 5 for the design of the construct). ChPheRS-1v1 and chPheRS-1v2 plasmids were generated using Gibson assembly with different lengths of *Mm*PylRS, a catalytic domain of *Hmt*PheRS, and the pcDNA3.1 backbone (see Figure 6A for the design of the construct). Mutations for chPheRS-3v2 (E391D) and for chPheRS-4v2 (F464V) were introduced into the chPheRS-1v2 sequence using site-directed mutagenesis. PMP(*Ec*LeuRS), PMP(*Ec*TyrRS), PMP(*Ec*TrpRS), and PMP(chPheRS-1v0) were cloned into the pcDNA3.1 backbone via Gibson assembly, fusing together LCK$_{1-10}$-FUS, MCP, and synthetase fragments. PMP(*Ma*PylRS) was inserted into the pcDNA3.1 backbone via Gibson assembly, fusing together LCK$_{1-10}$-FUS-MCP and *Ma*PylRS fragments. PMP(NES-*Ma*PylRS) plasmid was introduced into the pcDNA3.1 backbone via Gibson assembly, fusing LCK$_{1-10}$-FUS, MCP-NES, and *Ma*PylRS fragments. PMP (2x*Ma*PylRS) and PMP(3x*Ma*PylRS) were cloned into the pcDNA3.1 backbone via Gibson assembly, fusing LCK$_{1-10}$-FUS-MCP-*Ma*PylRS fragment with one or two copies of *Ma*PylRS, respectively. PMP(chPheRS-1v1) and PMP (chPheRS-1v2) were inserted into the pcDNA3.1 backbone via Gibson assembly, fusing LCK$_{1-10}$-FUS-MCP-*Mm*PylRS fragment (with various lengths of *Mm*PylRS, see Figure 6A for the design of the synthetases) and the catalytic domain of *Hmt*PheRS (with mutations T467G and A507G). PMP(chPheRS-3v2), and PMP(chPheRS-4v2) plasmids were generated via insertion of the catalytic domain of *Hmt*PheRS with the desired set of mutations (E391D, T467G, and A507G for chPheRS-3v2 and F464V, T467G and A507G for chPheRS-4v2, respectively) into the LCK$_{1-10}$-FUS-MCP-*Mm*PylRS (replacing fragments with various lengths in *Mm*PylRS, Figure 6A) using restriction cloning. The NLS-GFP^{39TAG}-ms2 reporter, employed for mass spectrometry validation of ncAA incorporation, was generated by transferring the open reading frame (ORF) from a previously reported construct in a pBI backbone[5,6] into the pcDNA3.1 backbone using restriction cloning. The plasmids NES-PylRS^{AF} (*Mm*PylRS), *Mm*tRNA^{Pyl}, iRFP-GFP^{39TAG}, NLS-GFP^{39TAG}-ms2, GFP^{39TAG}, mCherry^{189TAG}-ms2, GFP^{39TAG}, mCherry^{189TAG}-boxB, LCK$_{1-10}$-EWSR1-4xλN22, and the organelle construct PMP(*Mm*PylRS) were previously reported[27,5,6] and directly used in this study for transient transfections. The protein sequences of synthetase constructs used in this study are presented in the file Supplementary Data 1. The DNA sequences of tRNA constructs used in this study are provided in the file Supplementary Data 2.

Transient transfections

For flow cytometry experiments, HEK293T cells were seeded in each well of a 24-well plate; each well was transfected with a total of 1200 ng of plasmid DNA, except wells for experiments with chPheRS constructs where a total of 1500 ng of plasmid DNA was used. Typically, for flow cytometry analyses for wells containing 300 ng suppressor tRNA plasmid, equal amounts of (1) a fluorescent reporter (iRFP-GFP^{39TAG}; GFP^{39TAG}, mCherry^{189TAG}-ms2; or GFP^{39TAG}, mCherry^{189TAG}-boxB reporter), (2) RS-containing plasmid, (3) suppressor tRNA plasmid, and 4) mock plasmid (pcDNA3.1_Zeo+) were mixed in 50 μL DMEM without phenol red. If 1, 10, 50, or 150 ng of suppressor tRNA plasmid were used, more mock plasmid was added to ensure a total plasmid mass of 1200 ng. For experiments with *Ec*tRNA^{Leu}-13 and PMP(*Ec*LeuRS), the following mix of plasmids was used: (1) 300 ng of fluorescent reporter (GFP^{39TAG}, mCherry^{189TAG}-ms2; or GFP^{39TAG}, mCherry^{189TAG}-boxB reporter), (2) 50 ng of *Ec*LeuRS plasmid or PMP(*Ec*LeuRS) construct, (3) 1, 10, 50, 150, or 300 ng of *Ec*tRNA^{Leu}-13 plasmid, (4) 550 ng of LCK$_{1-10}$-EWSR1-4xλN22 construct and (5) mock plasmid (pcDNA3.1_Zeo+) to adjust total plasmid mass to 1200 ng if needed; the mix was prepared in 50 μL DMEM without phenol red. For experiments with chPheRS constructs, plasmids were mixed in 50 μL DMEM without phenol red: (1) 300 ng of dual-amber reporter (GFP^{39TAG}, mCherry^{189TAG}-ms2), (2) 600 ng of chPheRS or *Mm*PylRS (used as a control) construct, and (3) 600 ng of chtRNA^{Phe} or *Mm*tRNA^{Pyl} (used as a control) plasmid. For reporter only controls in flow cytometry experiments, 300 ng of the particular reporter used for the experiment were mixed with 900 ng (or 1200 ng for chPheRS experiments) mock plasmid (pcDNA3.1_Zeo+) in 50 μL DMEM without phenol red. For entire mock transfections in flow cytometry experiments, 1200 ng (or 1500 ng for chPheRS experiments) mock plasmid (pcDNA3.1_Zeo+) were added to 50 μL DMEM without phenol red. For IF labeling/tRNA FISH experiments, HEK293T cells were seeded in each well of a 4-well cell imaging cover glass, each well was transfected with a total of 1680 ng of plasmid DNA. Equal amounts of (1) NLS-GFP^{39TAG}-ms2 reporter, (2) PMP construct with introduced synthetase, (3) suppressor tRNA plasmid, and (4) mock plasmid (pcDNA3.1_Zeo+) were mixed in 70 μL DMEM without phenol red. For tRNA FISH control samples, suppressor tRNA plasmid was

replaced with the mock plasmid (pcDNA3.1_Zeo+). For mass spectrometry experiments, HEK293T cells seeded in each 100 mm round cell culture dish were transfected with a total of 30 μg of plasmid DNA. Equal amounts of (1) NLS-GFP^{39TAG}-ms2 reporter, (2) PMP construct with introduced synthetase, and (3) suppressor tRNA plasmid were mixed in 1 mL DMEM without phenol red. Polyethylenimine (PEI, 1 μg/μL, Sigma 408727-100 ml) was added to all transfections at a DNA/PEI ratio of 1:3. The mixtures were vortexed for 10 s, spun for 5 s, and incubated for 15 min at room temperature before being added dropwise into the wells. After 4 h, the medium in each well was removed and replaced with fresh medium buffered with 25 mM HEPES (pH 7.25). Samples incubated in the presence of ncAA contained in the buffered medium one of the next compounds: (1) 250 μM N^6-((cyclooct-2-yn-1-yloxy)carbonyl)-L-lysine (SCO-K, **1**, SiChem SC-8000) (or 62.5/15.6/3.9/1/0.24 μM in the experiment with the ncAA titration), (2) 250 μM 4,5-dimethoxy-2-nitrobenzylcysteine (DMNB-C, **2**, a kind gift from the Peter Schultz group (The Scripps Research Institute, La Jolla, USA)), (3) 250 μM p-benzoyl-L-phenylalanine (pBPA, **3**, Iris Biotech HAA6010.0005), (4) 250 μM 5-hydroxy-L-tryptophan (5HTP, **4**, Sigma-Aldrich H9772), (5) 2 mM p-azidophenylalanine (pAzF, **5**, Bachem F-3075.0001), (6) 2 mM 6-methyltryptophan (6MeTP, **6**, BLDPharm BD562299), (7) 2 mM 7-methyltryptophan (7MeTP, **7**, BLDPharm BD562297).

Flow cytometry and data analysis

HEK293T cells were cultured for 24 h after the change of medium and then harvested for flow cytometry analysis. First, cells were rinsed once with 200 μL of 1x PBS, then detached using 100 μL of trypsin-EDTA solution (0.05% concentration, with phenol red, Gibco, 25300-054) and incubated at 37 °C and 5% CO_2 for 5 min. Subsequently, 900 μL of resuspension buffer 1 (1x PBS with 10% FBS, 2 mM sodium azide, and 2 mM EDTA) was added to each well. The cells were then collected on ice, transferred to 1.5 mL tubes, and pelleted for 5 min at 400*g* and 4 °C. The supernatants were discarded, and the cell pellets were washed with 900 μL of resuspension buffer 2 (1x PBS with 3% bovine serum albumin (BSA), 2 mM sodium azide, and 2 mM EDTA). The cells were again centrifuged for 5 min at 400*g* and 4 °C. After discarding the supernatants, 250 μL of resuspension buffer 2 was added to cell pellets. The cells were then resuspended, and a total 300 μL aliquot of the cell suspension was further used for flow cytometry analysis. To enable live cell staining, 3 μL of DAPI (50 μg/mL) were added to the cell suspension. The samples were incubated on ice for 1–2 min before measurement. Data acquisition was carried out using an LSRFortessa Cell Analyzer (BD Biosciences). Data analysis was performed using FlowJo version 10.7.1 (BD Biosciences). As a first step in the gating strategy (Supplementary Figures 30 and 31), the HEK293T cell population was selected based on FSC-A x SSC-A parameters. Next, single cell population was gated using SSC-W x SSC-A parameters. Finally, live cells were picked based on SSC-W x 405–450/50 channel parameters. At least 100,000 live cells were collected and analyzed for each measured sample. Further analysis was dependent on the reporter used for the particular experiment:

FC analysis of the dual-amber fluorescent reporter (GFP^{39TAG}, mCherry^{189TAG}-ms2). The fluorescence of GFP was acquired using a 488 nm laser and a 530/30 bandpass filter. For detecting mCherry, a 561 nm laser with a 610/20 bandpass filter was used. Measurements of live cells were plotted with GFP fluorescence on the OX axis and mCherry fluorescence on the OY axis. The plot was divided into two quadrants. The workflow of cell gating is shown in Supplementary Figure 30. To calculate median mCherry signal and median GFP signal, only cells from the top half were selected. Microsoft Excel files containing median mCherry and median GFP values were generated from the FlowJo workspace and used for calculating fold change selectivity, relative efficiency^{mCherry} (%), and relative efficiency^{GFP} (%). Fold change selectivity was quantified as the median mCherry signal divided by the median GFP signal of a given system normalized to the respective ratio for the control with non-organelle-fused synthetase. Percentage relative efficiency^{mCherry} to assess GCE efficiency in OT organelles was calculated as the median mCherry signal of a sample with an OT organelle system divided by the median mCherry signal of sample with corresponding non-organelle-fused synthetase. Percentage relative efficiency^{mCherry} for Supplementary Figure 24 was calculated for chPheRS experiments as the median mCherry signal of a studied sample divided by the median mCherry signal for the sample where chPheRS-1v0 was used for the amber suppression. Percentage relative efficiency^{GFP} was calculated for chPheRS experiments as the median GFP signal of a given system divided by the median GFP signal for the sample where chPheRS-1v0 was used for the amber suppression. Three biological replicates were performed for chPheRS experiments; for all other experiments, one biological replicate was carried out. Values for the fold change selectivity and the percentage relative efficiencies were calculated in Microsoft Excel and transferred to Prism software (GraphPad). Mean values and standard deviation were quantified if three replicates were performed for the experiment, and then the corresponding bar plots

were generated. For the experiments with one performed biological replicate, the relative efficiencies were calculated in Microsoft Excel and transferred to Prism software (GraphPad) to generate the corresponding bar plots.

FC analysis of iRFP-GFP^{39TAG} reporter. The fluorescence of GFP was acquired using a 488 nm laser and a 530/30 bandpass filter. For detecting iRFP, a 640 nm laser with a 730/45 bandpass filter was used. Measurements of live cells were plotted with GFP fluorescence on the OX axis and iRFP fluorescence on the OY axis. The plot was divided into four quadrants. The workflow of cell gating is shown in Supplementary Figure 31. To calculate median GFP signal and to obtain percentage of GFP+ cells, only cells from the top-right quadrant (Q2) were considered. For quantification of the median iRFP signal and percentage of iRFP+ cells, cells from the two top quadrants (top left and top right, Q1 and Q2, respectively) were selected. Microsoft Excel files containing median iRFP and GFP values and percentage of GFP+ and iRFP+ cells were generated from the FlowJo workspace and used for calculating relative efficiency (median) (%) and relative efficiency (abundance) (%). Percentage relative efficiency (median) was calculated as the median GFP signal for each particular sample divided by the median iRFP signal for the same sample and normalized to the sample where *Ec*tRNA^{Leu} WT was transfected without RNA-binding protein, which is equal to 100%. Percentage relative efficiency (abundance) was calculated as the percentage of GFP+ cells for each particular sample divided by the percentage of iRFP+ cells for the same sample and normalized to the sample where *Ec*tRNA^{Leu} WT was transfected without RNA-binding protein, which is equal to 100%. One biological experiment was performed for all experiments. The relative efficiencies were calculated in Microsoft Excel and transferred to Prism software (GraphPad) to generate the corresponding bar plots.

Immunofluorescence (IF) labeling, tRNA FISH, and confocal imaging

After changing the medium, HEK293T cells were incubated for 24 h at 37 °C and 5% CO_2 in the presence of complementary ncAA, then rinsed once with 1x PBS and fixed using 700 μL 4% formaldehyde in 1x PBS for 1 h at room temperature. After fixation, the fixation solution was discarded, and the cells were rinsed once with 1x PBS and permeabilized with 450 μL 0.5% Triton X-100 in 1x PBS for 15 min at room temperature. Then, the permeabilization solution was removed, the cells were rinsed once with 1x PBS and incubated with 700 μL 2x SSC buffer (0.3 M NaCl, 30 mM sodium citrate, pH = 7.4) in 50% formamide for 5 min at room temperature. After that, the 2x SSC buffer was discarded, and 450 μL hybridization buffer with a FISH probe was added to the samples. The hybridization buffer contained 4x SSC buffer (0.6 M NaCl, 60 mM sodium citrate, pH = 7.4), 50% formamide, 100 μg/μL dextran sulfate (Sigma-Aldrich, D8906), 198 ng/μL BSA, 2 mM VRC (ribonucleoside vanadyl complexes, Sigma-Aldrich, 94740), 80 ng/μL *E. coli* tRNA (Sigma-Aldrich, R1753) for *Mm*PylRS/*Mm*tRNA^{Pyl} and *Ma*PylRS/*Ma*tRNA^{Pyl} pairs or 80 ng/μL baker's yeast (*S. cerevisiae*) tRNA (Sigma-Aldrich, R8759) for *Ec*LeuRS/*Ec*tRNA^{Leu}, *Ec*TyrRS/*Bst*tRNA^{Tyr}, and *Ec*TrpRS/*Ec*tRNA^{Trp} pairs, and 0.5 μM 5′-Cy5 labeled oligonucleotide complementary to the studied suppressor tRNA (FISH probe). The following FISH probes were used in this study: (1) 5′-Cy5-C TAACCCGGCTGAACGGATTTAGAGTCCATTC GATC-3′ – for *Mm*tRNA^{Pyl}, (2) 5′-Cy5-GATTTAGAATCCCTTG TGTCTACCGATTC CACC-3′ – for *Ec*tRNA^{Leu}, (3) 5′-Cy5-GGATTTA GAGTCCGCCGCGTTTAGC-3′ – for *Bst*tRNA^{Tyr}, (4) 5′-Cy5-GGTTTTAGAGACCGGTGCTCTAC CAATTGAACTACGC-3′ – for *Ec*tRNA^{Trp}, (5) 5′-Cy5-CTAGGTTTTAGAGACCCGCTGGTCG-3′ – for *Ma*tRNA^{Pyl}. The samples were incubated with the hybridization buffer overnight at 37 °C. Next day, the hybridization buffer was removed, and the cells were subsequently washed with 700 μL 4x SSC buffer (0.6 M NaCl, 60 mM sodium citrate, pH = 7.4) in 50% formamide, 700 μL 2x SSC buffer (0.3 M NaCl, 30 mM sodium citrate, pH = 7.4) in 50% formamide, 700 μL 1x SSC buffer (0.15 M NaCl, 15 mM sodium citrate, pH = 7.4) in 50% formamide, 700 μL 0.5x SSC buffer (75 mM NaCl, 7.5 mM sodium citrate, pH = 7.4) in 50% formamide, and 700 μL Tris-HCl·NaCl buffer (0.1 M Tris-HCl, 150 mM NaCl, pH = 7.5); at each wash step the cells were incubated with washing buffers for 5 min at room temperature. After that, the cells were blocked using 450 μL 3% BSA in 1x PBS for 1.5 h at room temperature. Then, the blocking buffer was discarded, and the cells were incubated with 450 μL mouse anti-HA antibody (Sigma-Aldrich, H9658, diluted 1:2000 in 3% BSA in 1x PBS) for 2 h at room temperature. After the incubation with the primary antibody, the mouse anti-HA antibody solution was removed, the cells were rinsed once with 1x PBS and further incubated with 450 μL goat anti-mouse antibody conjugated with Cy3 (Thermo Fisher Scientific, A10521, diluted 1:1000 in 3% BSA in 1x PBS) for 1 h at room temperature. After the incubation with the secondary antibody, the goat anti-mouse antibody solution was discarded, the cells were rinsed once with 1x PBS, and finally, 700 μL 1x PBS was added to the samples. The cells were imaged using Leica TCS SP5 confocal microscope with 488 nm (for GFP), 561 nm (for Cy3), and 633 nm

(for Cy5) lasers for excitation and 63x/1.40 oil immersion objective. Laser powers were varied for different RS/tRNA pairs to obtain appropriate images for assessment of OTO, tRNA, and NES-GFP localization. The images were captured using the LAS AF software (Leica). Data analysis of images was later performed using ImageJ (Fiji).[54] Different contrast adjustments were applied for distinct RS/tRNA pairs during image analysis to obtain the best possible visualization of OTOs, tRNAs, and NES-GFP. One biological replicate was carried out for the IF/tRNA FISH experiment.

Mass spectrometry analyses

Cell harvesting. 48 h after the addition of the ncAA, the medium was removed from the cells, which were then washed with 1x PBS and detached using trypsin-EDTA solution. The cells were centrifuged at 400*g* for 5 min, and the resulting cell pellet was shock-frozen in liquid nitrogen and stored at −80 °C for further processing.

Cell lysis and GFP enrichment. The cell pellets were lysed in 200 μL of RIPA buffer (10 mM Tris/HCl pH 7.5, 150 mM NaCl, 0.5 mM EDTA, 0.1% SDS, 1% Triton™ X-100, 1% deoxycholate, 1x complete protease inhibitor, 1 mM $MgCl_2$, 1 mM PMSF, 6.75 mU/μL Sm-nuclease) and incubated on ice for 30 min. Following this, dilution buffer (10 mM Tris/HCl pH 7.5, 150 mM NaCl, 0.5 mM EDTA, 1x complete protease inhibitor, 1 mM PMSF) was added. GFP-Trap® Magnetic Agarose (Chromotek, gtma-100) equilibrated in dilution buffer (25 μL slurry) was then added to the lysate. The mixture was subjected to end-over-end rotation at 4 °C for 1 h. The beads were washed three times with 500 μL of wash buffer (10 mM Tris/Cl pH 7.5, 150 mM NaCl, 0.05% Nonidet™ P40 Substitute, 0.5 mM EDTA), resuspended in 10 μL RIPA buffer and 10 μL 2x SDS sample buffer (120 mM Tris/Cl pH 6.8, 20% glycerol, 4% SDS, 0.04% bromophenol blue, 10% β-mercaptoethanol).

GFP elution and SDS-PAGE. For elution, the beads were boiled at 95 °C for 5 min, and the supernatant was loaded onto a NuPAGE™ 4–12% Bis-Tris gel (1.0 mm) (Invitrogen, NP0321BOX). Electrophoresis was performed at 200 V for 45 min. The gel was then stained with 1x Coomassie Brilliant Blue and destained overnight in ddH2O. The band at the expected molecular weight was excised and prepared for mass spectrometry analysis.

Protein in-gel digestion. Coomassie-stained protein gel bands were cut into small cubes, followed by destaining in 50% ethanol/25 mM ammonium bicarbonate. Afterward, proteins were reduced in 10 mM DTT at 56 °C and alkylated by 50 mM iodoacetamide in the dark at room temperature. Enzymatic digestion of proteins was performed using trypsin alone or a combination of trypsin and Glu-C in 50 mM ammonium bicarbonate overnight at 37 °C. Following peptide extraction sequentially using 30% and 100% acetonitrile, the sample volume was reduced in a centrifugal evaporator to remove residual acetonitrile. The resultant peptide solution was purified by solid phase extraction in C18 StageTips (PMID: 12585499).

LC-MS/MS analysis of NLS-GFP^{39pAzF}, NLS-GFP$^{39\ 6MeTP}$ and NLS-GFP$^{39\ 7MeTP}$. Peptides were separated in an in-house packed 45-cm analytical column (inner diameter: 75 μm; ReproSil-Pur 120 C18-AQ 1.9-μm beads, Dr. Maisch GmbH) by online reverse phase liquid chromatography through a 90-min non-linear gradient of 2.4–32% acetonitrile with 0.1% formic acid at a nanoflow rate of 250 nL/min. The eluted peptides were sprayed directly by electrospray ionization into an Exploris 480 Orbitrap mass spectrometer (Thermo Scientific). Mass spectrometry measurement was conducted in data-dependent acquisition mode using a top15 method with one full scan (mass range: 325 to 1,300 *m*/*z*; resolution: 60,000, target value: 3×10^6, maximum injection time: 28 ms) followed by 15 fragmentation scans via higher energy collision dissociation (HCD; normalized collision energy: 30%, resolution: 15,000, target value: 1×10^5, maximum injection time: 40 ms, isolation window: 1.4 *m*/*z*). Precursor ions of unassigned, +1, or higher than +6 charge state were rejected. Additionally, precursor ions already isolated for fragmentation were dynamically excluded for 25 s.

Mass spectrometry data processing. Raw data files were processed by MaxQuant software (version 2.1.3.0) (PMID: 19029910) using its built-in Andromeda search engine (PMID: 21254760). Spectral data were searched against a target-decoy database consisting of the forward and reverse sequences of GFP reporter protein variants whose residue position 39 is the unnatural pAzF, 6MeTP or 7MeTP (O as a place holder), p-aminophenylalanine (pAmF; U as a place holder) or any one of the 20 natural amino acids, the UniProt human reference proteome (release 2022_03; 101,761 entries) and a default list of common contaminants. Trypsin/P or Trypsin/P + GluC specificity was assigned to the corresponding raw files. Carbamidomethylation of cysteine, pyrrolysine to pAzF, 6MeTP, or 7MeTP substitution, and the corresponding selenocysteine to pAmF substitution were set as fixed modification. Oxidation of methionine and acetylation of the protein N-terminus were chosen as variable modifications. A maximum of 2 missed

cleavages were tolerated. The minimum peptide length was set to be 7 amino acids. False discovery rate (FDR) was set to 1% for both peptide and protein identifications. The processed MS/MS spectra were visualized and annotated in the Viewer module of MaxQuant (PMID: 25644178).

DECLARATION OF COMPETING INTEREST

The authors declare the following financial interests/personal relationships which may be considered as potential competing interests: "E.A. L. holds patents related to OTOs. M.E.S. and M.J. declare no competing interests.".

Acknowledgements

We thank all the members of the Lemke laboratory for their helpful discussions. We thank the Flow Cytometry Core Facility, Proteomics Core Facility, and Microscopy Core Facility at the Institute of Molecular Biology (IMB) for expert assistance. E.A.L. acknowledges funding from the Volkswagenstiftung (Life) as well as CRC1551' Polymer concepts in cellular function' of the Deutsche Forschungsgemeinschaft (DFG project number 464588647).

Appendix A. Supplementary material

Supplementary material to this article can be found online at https://doi.org/10.1016/j.jmb.2024.168728.

Received 8 June 2024;
Accepted 25 July 2024;
Available online 30 July 2024

Keywords:
genetic code expansion;
noncanonical amino acid;
orthogonally translating organelles;
phase separation;
protein engineering

References

1. Liu, C.C., Schultz, P.G., (2010). Adding new chemistries to the genetic code. *Annu. Rev. Biochem.* **79**, 413–444.
2. Lemke, E.A., (2014). The exploding genetic code. *ChemBioChem* **15**, 1691–1694.
3. Chin, J.W., (2017). Expanding and reprogramming the genetic code. *Nature* **550**, 53–60.
4. de la Torre, D., Chin, J.W., (2021). Reprogramming the genetic code. *Nature Rev. Genet.* **22**, 169–184.
5. Reinkemeier, C.D., Girona, G.E., Lemke, E.A., (2019). Designer membraneless organelles enable codon reassignment of selected mRNAs in eukaryotes. *Science* **363**, eaaw2644
6. Reinkemeier, C.D., Lemke, E.A., (2021). Dual film-like organelles enable spatial separation of orthogonal eukaryotic translation. *Cell* **184**, 4886–4903.e21.
7. Reinkemeier, C.D., Lemke, E.A., (2022). Condensed, microtubule-coating thin organelles for orthogonal translation in mammalian cells. *J. Mol. Biol.* **434**, 167454.
8. Yu, M., Heidari, M., Mikhaleva, S., Tan, P.S., Mingu, S., Ruan, H., Reinkemeier, C.D., Obarska-Kosinska, A., Siggel, M., Beck, M., Hummer, G., Lemke, E.A., (2023). Visualizing the disordered nuclear transport machinery in situ. *Nature* **617**, 162–169.
9. Nikić, I., Plass, T., Schraidt, O., Szymański, J., Briggs, J.A. G., Schultz, C., Lemke, E.A., (2014). Minimal tags for rapid dual-color live-cell labeling and super-resolution microscopy. *Angew. Chem. Int. Ed.* **53**, 2245–2249.
10. Uttamapinant, C., Howe, J.D., Lang, K., Beránek, V., Davis, L., Mahesh, M., Barry, N.P., Chin, J.W., (2015). Genetic code expansion enables live-cell and super-resolution imaging of site-specifically labeled cellular proteins. *J. Am. Chem. Soc.* **137**, 4602–4605.
11. Koehler, C., Sauter, P.F., Wawryszyn, M., Girona, G.E., Gupta, K., Landry, J.J.M., Fritz, M.H.Y., Radic, K., Hoffmann, J.E., Chen, Z.A., Zou, J., Tan, P.S., Galik, B., Junttila, S., Stolt-Bergner, P., Pruneri, G., Gyenesei, A., Schultz, C., Biskup, M.B., Besir, H., Benes, V., Rappsilber, J., Jechlinger, M., Korbel, J.O., Berger, I., Braese, S., Lemke, E.A., (2016). Genetic code expansion for multiprotein complex engineering. *Nature Methods* **13**, 997–1000.
12. Koehler, C., Sauter, P.F., Klasen, B., Waldmann, C., Pektor, S., Bausbacher, N., Lemke, E.A., Miederer, M., (2023). Genetic code expansion for site-specific labeling of antibodies with radioisotopes. *ACS Chem. Biol.* **18**, 443–448.
13. Lemke, E.A., Summerer, D., Geierstanger, B.H., Brittain, S.M., Schultz, P.G., (2007). Control of protein phosphorylation with a genetically encoded photocaged amino acid. *Nature Chem. Biol.* **3**, 769–772.
14. Elsässer, S.J., Ernst, R.J., Walker, O.S., Chin, J.W., (2016). Genetic code expansion in stable cell lines enables encoded chromatin modification. *Nature Methods* **13**, 158–164.
15. Davis, L., Chin, J.W., (2012). Designer proteins: applications of genetic code expansion in cell biology. *Nature Rev. Mol. Cell Biol.* **13**, 168–182.
16. Nikić-Spiegel, I., (2020). Expanding the genetic code for neuronal studies. *ChemBioChem* **21**, 3169–3179.
17. Shandell, M.A., Tan, Z., Cornish, V.W., (2021). Genetic code expansion: a brief history and perspective. *Biochemistry* **60**, 3455–3469.
18. Bertrand, E., Chartrand, P., Schaefer, M., Shenoy, S.M., Singer, R.H., Long, R.M., (1998). Localization of ASH1 mRNA particles in living yeast. *Mol. Cell* **2**, 437–445.
19. Wu, N., Deiters, A., Cropp, T.A., King, D., Schultz, P.G., (2004). A genetically encoded photocaged amino acid. *J. Am. Chem. Soc.* **126**, 14306–14307.
20. Young, T.S., Ahmad, I., Brock, A., Schultz, P.G., (2009). Expanding the genetic repertoire of the methylotrophic yeast *Pichia pastoris*. *Biochemistry* **48**, 2643–2653.

21. Kang, J.-Y., Kawaguchi, D., Coin, I., Xiang, Z., O'Leary, D. D.M., Slesinger, P.A., Wang, L., (2013). In vivo expression of a light-activatable potassium channel using unnatural amino acids. *Neuron* **80**, 358–370.
22. Sakamoto, K., Hayashi, A., Sakamoto, A., Kiga, D., Nakayama, H., Soma, A., Kobayashi, T., Kitabatake, M., Takio, K., Saito, K., Shirouzu, M., Hirao, I., Yokoyama, S., (2002). Site-specific incorporation of an unnatural amino acid into proteins in mammalian cells. *Nucleic Acids Res.* **30**, 4692–4699.
23. Chin, J.W., Cropp, T.A., Anderson, J.C., Mukherji, M., Zhang, Z., Schultz, P.G., (2003). An expanded eukaryotic genetic code. *Science* **301**, 964–967.
24. Italia, J.S., Addy, P.S., Wrobel, C.J.J., Crawford, L.A., Lajoie, M.J., Zheng, Y., Chatterjee, A., (2017). An orthogonalized platform for genetic code expansion in both bacteria and eukaryotes. *Nature Chem. Biol.* **13**, 446–450.
25. Willis, J.C.W., Chin, J.W., (2018). Mutually orthogonal pyrrolysyl-tRNA synthetase/tRNA pairs. *Nature Chem.* **10**, 831–837.
26. Meineke, B., Heimgärtner, J., Lafranchi, L., Elsässer, S.J., (2018). *Methanomethylophilus alvus Mx1201* provides basis for mutual orthogonal pyrrolysyl tRNA/aminoacyl-tRNA synthetase pairs in mammalian cells. *ACS Chem. Biol.* **13**, 3087–3096.
27. Nikic, I., Kang, J.H., Girona, G.E., Aramburu, I.V., Lemke, E.A., (2015). Labeling proteins on live mammalian cells using click chemistry. *Nature Protoc.* **10**, 780–791.
28. Seki, E., Yanagisawa, T., Kuratani, M., Sakamoto, K., Yokoyama, S., (2020). Fully productive cell-free genetic code expansion by structure-based engineering of *Methanomethylophilus alvus* pyrrolysyl-tRNA synthetase. *ACS Synth. Biol.* **9**, 718–732.
29. Herring, S., Ambrogelly, A., Gundllapalli, S., O'Donoghue, P., Polycarpo, C.R., Söll, D., (2007). The amino-terminal domain of pyrrolysyl-tRNA synthetase is dispensable in vitro but required for in vivo activity. *FEBS Lett.* **581**, 3197–3203.
30. Tan, M., Wang, M., Zhou, X.L., Yan, W., Eriani, G., Wang, E.D., (2013). The Yin and Yang of tRNA: Proper binding of acceptor end determines the catalytic balance of editing and aminoacylation. *Nucleic Acids Res.* **41**, 5513–5523.
31. Jakes, R., Fersht, A.R., (1975). Tyrosyl-tRNA synthetase from *Escherichia coli*. Stoichiometry of ligand binding and half-of-the-sites reactivity in aminoacylation. *Biochemistry* **14**, 3344–3350.
32. Ibba, M., Sever, S., Praetorius-Ibba, M., Söll, D., (1999). Transfer RNA identity contributes to transition state stabilization during aminoacyl-tRNA synthesis. *Nucleic Acids Res.* **27**, 3631–3637.
33. Yanagisawa, T., Ishii, R., Fukunaga, R., Kobayashi, T., Sakamoto, K., Yokoyama, S., (2008). Multistep engineering of pyrrolysyl-tRNA synthetase to genetically encode Nε-(o-azidobenzyloxycarbonyl) lysine for site-specific protein modification. *Chem. Biol.* **15**, 1187–1197.
34. Guo, L.-T., Wang, Y.-S., Nakamura, A., Eiler, D., Kavran, J. M., Wong, M., Kiessling, L.L., Steitz, T.A., O'Donoghue, P., Söll, D., (2014). Polyspecific pyrrolysyl-tRNA synthetases from directed evolution. *Proc. Natl. Acad. Sci. U.S.A.* **111**, 16724–16729.
35. Hamano-Takaku, F., Iwama, T., Saito-Yano, S., Takaku, K., Monden, Y., Kitabatake, M., Söll, D., Nishimura, S., (2000). A mutant *Escherichia coli* tyrosyl-tRNA synthetase utilizes the unnatural amino acid azatyrosine more efficiently than tyrosine. *J. Biol. Chem.* **275**, 40324–40328.
36. Zúñiga, R., Salazar, J., Canales, M., Orellana, O., (2002). A dispensable peptide from Acidithiobacillus ferrooxidans tryptophanyl-tRNA synthetase affects tRNA binding. *FEBS Lett.* **532**, 387–390.
37. Guo, L.-T., Amikura, K., Jiang, H.-K., Mukai, T., Fu, X., Wang, Y.-S., O'Donoghue, P., Söll, D., Tharp, J.M., (2022). Ancestral archaea expanded the genetic code with pyrrolysine. *J. Biol. Chem.* **298**, 102521.
38. Suzuki, T., Miller, C., Guo, L.T., Ho, J.M.L., Bryson, D.I., Wang, Y.S., Liu, D.R., Söll, D., (2017). Crystal structures reveal an elusive functional domain of pyrrolysyl-tRNA synthetase. *Nature Chem. Biol.* **13**, 1261–1266.
39. Yamaguchi, A., Iraha, F., Ohtake, K., Sakamoto, K., (2018). Pyrrolysyl-tRNA synthetase with a unique architecture enhances the availability of lysine derivatives in synthetic genetic codes. *Molecules* **23**, 2460.
40. Nikić, I., Estrada Girona, G., Kang, J.H., Paci, G., Mikhaleva, S., Koehler, C., Shymanska, N.V., Ventura Santos, C., Spitz, D., Lemke, E.A., (2016). Debugging eukaryotic genetic code expansion for site-specific Click-PAINT super-resolution microscopy. *Angew. Chem. Int. Ed.* **55**, 16172–16176.
41. Chattopadhyay, S., Garcia-Mena, J., DeVito, J., Wolska, K., Das, A., (1995). Bipartite function of a small RNA hairpin in transcription antitermination in bacteriophage lambda. *Proc. Natl. Acad. Sci. u.s.a.* **92**, 4061–4065.
42. Daigle, N., Ellenberg, J., (2007). λN-GFP: An RNA reporter system for live-cell imaging. *Nature Methods* **4**, 633–636.
43. Asahara, H., Nameki, N., Hasegawa, T., (1998). In vitro selection of RNAs aminoacylated by *Escherichia coli* leucyl-tRNA synthetase. *J. Mol. Biol.* **283**, 605–618.
44. Lim, F., Downey, T.P., Peabody, D.S., (2001). Translational repression and specific RNA binding by the coat protein of the *Pseudomonas* phage PP7. *J. Biol. Chem.* **276**, 22507–22513.
45. Larson, D.R., Zenklusen, D., Wu, B., Chao, J.A., Singer, R. H., (2011). Real-time observation of transcription initiation and elongation on an endogenous yeast gene. *Science* **332**, 475–478.
46. Mukai, T., (2020). Rational design of aptamer-tagged tRNAs. *Int. J. Mol. Sci.* **21**, 7793.
47. Ding, W., Zhao, H., Chen, Y., Zhang, B., Yang, Y., Zang, J., Wu, J., Lin, S., (2020). Chimeric design of pyrrolysyl-tRNA synthetase/tRNA pairs and canonical synthetase/tRNA pairs for genetic code expansion. *Nature Commun.* **11**, 3154.
48. Bryson, D.I., Fan, C., Guo, L.-T., Miller, C., Söll, D., Liu, D. R., (2017). Continuous directed evolution of aminoacyl-tRNA synthetases. *Nature Chem. Biol.* **13**, 1253–1260.
49. Klipcan, L., Moor, N., Finarov, I., Kessler, N., Sukhanova, M., Safro, M.G., (2012). Crystal structure of human mitochondrial PheRS complexed with $tRNA^{Phe}$ in the active "open" state. *J. Mol. Biol.* **415**, 527–537.
50. Zhao, H., Ding, W., Zang, J., Yang, Y., Liu, C., Hu, L., Chen, Y., Liu, G., Fang, Y., Yuan, Y., Lin, S., (2021). Directed-evolution of translation system for efficient unnatural amino acids incorporation and generalizable synthetic auxotroph construction. *Nature Commun.* **12**, 7039.
51. Greiss, S., Chin, J.W., (2011). Expanding the genetic code of an animal. *J. Am. Chem. Soc.* **133**, 14196–14199. https://doi.org/10.1021/ja2054034.

52. Parrish, A.R., She, X., Xiang, Z., Coin, I., Shen, Z., Briggs, S.P., Dillin, A., Wang, L., (2012). Expanding the genetic code of *Caenorhabditis elegans* using bacterial aminoacyl-tRNA synthetase/tRNA Pairs. *ACS Chem. Biol.* **7**, 1292–1302. https://doi.org/10.1021/cb200542j.
53. Sushkin, M.E., Koehler, C., Lemke, E.A., (2023). Remodeling the cellular stress response for enhanced genetic code expansion in mammalian cells. *Nature Commun.* **14**, 6931. https://doi.org/10.1038/s41467-023-42689-2.
54. Schindelin, J., Arganda-Carreras, I., Frise, E., Kaynig, V., Longair, M., Pietzsch, T., Preibisch, S., Rueden, C., Saalfeld, S., Schmid, B., Tinevez, J.-Y., White, D.J., Hartenstein, V., Eliceiri, K., Tomancak, P., Cardona, A., (2012). Fiji: an open-source platform for biological-image analysis. *Nature Methods* **9**, 676–682.